Taylor, B., Fujioka, K., et al., 1992
Proceedings of the Ocean Drilling Program, Scientific Results, Vol. 126

2. CORRELATION OF QUATERNARY TEPHRAS THROUGHOUT THE IZU-BONIN AREAS[1]

Kantaro Fujioka,[2] Akira Nishimura,[3] Yoshiko Matsuo,[4] and Kelvin S. Rodolfo[5]

ABSTRACT

Quaternary marine tephras in the Izu-Bonin Arc offer significant information about explosive volcanic activities of the arc. Visual core descriptions, petrographic examinations, and chemical and grain-size analyses were conducted on tephras of backarc, arc, and forearc origin. Tephras are black and white and occur in simple and multiple modes with mixed and nonmixed ashes of black and white glass shards. The grain size distributions of the tephras are classified into three categories: coarse, white pumiceous, and fine white and black well-sorted types. The frequency of occurrence of the white and black tephras differs within the tectonic settings of the arc. Chemically, the Quaternary tephras in this region belong to low-alkali tholeiitic series with lower K_2O and TiO_2 than normal ordinary arc volcanic materials. Several tephras from different sites along the forearc correlate with each other and with tephras in the Shikoku Basin site and with Aogashima volcanics. These volcanic ashes resemble those in other backarc rifting areas, such as in the Fiji, Okinawa (Ryukyu), and Mariana regions.

INTRODUCTION

The distribution of Quaternary marine tephras around the Japanese Islands has been well documented by studies of piston core samples taken in the region (Machida and Arai, 1983, 1988; Furuta et al., 1986). However, tephras along the Izu-Bonin Arc are not as well studied, except for those of Oshima Island, south of Tokyo (Nakamura, 1964). Drilling along the Izu-Bonin Arc provides an excellent opportunity to document the chemistry and distribution of these opean-ocean tephras and to correlate them, if possible, to those around the Japanese Islands. Moreover, obtaining information on the volcanic ash layers along the Izu-Bonin Arc is of primary importance for understanding the tectonic evolution of the arc.

During Ocean Drilling Program (ODP) Leg 126, we recovered a large number of tephra layers from the Aogashima and Sumisujima area in the Izu-Bonin Arc south of Hachijojima Island, several hundred kilometers from Tokyo. Seven sites were drilled around the active volcanic islands of Aogashima and Sumisujima: three sites in the forearc basin (Sites 787, 792, and 793), two sites on the volcanic front (Sites 788 and 789), and two sites in the active backarc Sumisu Rift (Sites 790 and 791), resulting in a cross-sectional traverse of the arc through the forearc to the backarc (Figs. 1 and 2).

Site 787 in the Aogashima canyon, Site 792 at the fork of the Aogashima canyon, and Site 793 in the middle part of the upper slope basin were drilled in the forearc of the Izu-Bonin Arc (Fig. 1). The three sites have similar Oligocene to Holocene lithologies (Fig. 3). Three major lithologic units are evident: gravity flow, hemipelagic sediments, and volcaniclastic materials (Taylor, Fujioka, et al., 1990). The sedimentation rates of the three units at each of these three sites are also identical to each other: high in the gravity flow facies, very low in the hemipelagic facies, and moderately high in the volcaniclastic facies (Taylor, Fujioka, et al., 1990). More than 300 tephra layers were successfully recovered from these three sites.

Site 788 was drilled on the footwall of the Sumisu backarc rift, a well-studied backarc rift of the Izu-Bonin Arc (Fujioka, 1983a, 1983b, 1988; Brown and Taylor, 1988; Murakami, 1988; Nishimura and Murakami, 1988; Yamazaki, 1988; Ikeda and Yuasa, 1989; Fujioka et al., 1990) (Fig. 4). At this site, thick pumiceous layers were recovered with Pliocene altered pumice beds at the base.

Sites 790 and 791 were drilled 2.5 km apart in the eastern half-graben of the eastern Sumisu Rift (Fig. 4). Three major lithologies, including basement basalts, were identified in these Sumisu Rift sites. The upper half of the section consists of coarse pumiceous beds with four or five cycles of coarse pumice units underlying thin nannofossil-rich hemipelagites. The basement of the rift basin was characterized by a frothy vesicular basalt similar in chemical composition to the backarc basin basalt (Gill et al., 1990; Taylor, Fujioka, et al., 1990; Leg 126 Shipboard Scientific Party, 1989; Leg 126 Scientific Drilling Party, 1989).

We recovered more than 500 volcanic ash layers and ashy intervals in the Quaternary sediments along the Izu-Bonin Arc during Leg 126. This report documents the chemical nature of these volcanic ash layers and the accumulation rate of the volcaniclastic materials in the region. We also summarize the features and timing of the explosive volcanism that took place along the Izu-Bonin Arc during the Quaternary.

METHODS

Smear Slide Observations

To determine the mineral assemblage, mode, and morphology of the glass shards and the nature of the lithic fragments of the volcanic ash layers, we made smear slides of each tephra unit following the procedure outlined in the explanatory notes of the Leg 126 *Initial Reports* volume (see Taylor, Fujioka, et al., 1990).

Grain-size Analysis

The grain-size distribution of the tephras were determined with a laser light grain-size analyzer for particles smaller than 500 µm; for those larger than 500 µm, the samples were first sieved, and then their weights were measured.

Materials finer than 44 µm were eliminated by sieving. The 500 µm fraction was analyzed with an automatic laser-beam particle analyzer (Model SALD 1100 of Shimadzu Co Ltd., Japan). Sediments were put into a glass vessel with distilled water. After being mixed in an ultrasonic cleaner for 10 s, the samples are put into the quartz cell of the laser unit. In this unit, laser light refracts suspended materials, and the ratio of the reflected light from particles inside the quartz cell are measured by a photodetector. The accuracy of the grain-size distribution for each tephra layer is more than 95%.

---

[1] Taylor, B., Fujioka, K., et al., 1992. *Proc. ODP, Sci. Results,* 126: College Station, TX (Ocean Drilling Program).

[2] Ocean Research Institute, University of Tokyo, 1-15-1 Minamidai, Nakano, Tokyo 164, Japan (present address: Japan Marine Science and Technology Center, 2-14 Natsushima, Yokosuka, Kanagowa 238, Japan).

[3] Marine Geology Department, Geological Survey of Japan, 1-1-3 Yatabe, Tsukuba 305, Japan.

[4] Institute of Geosciences, Shizuoka University, 836 Oya, Shizuoka 422, Japan.

[5] Department of Geological Sciences, University of Illinois at Chicago, P.O. Box 4348, Chicago, IL 60680, U.S.A.

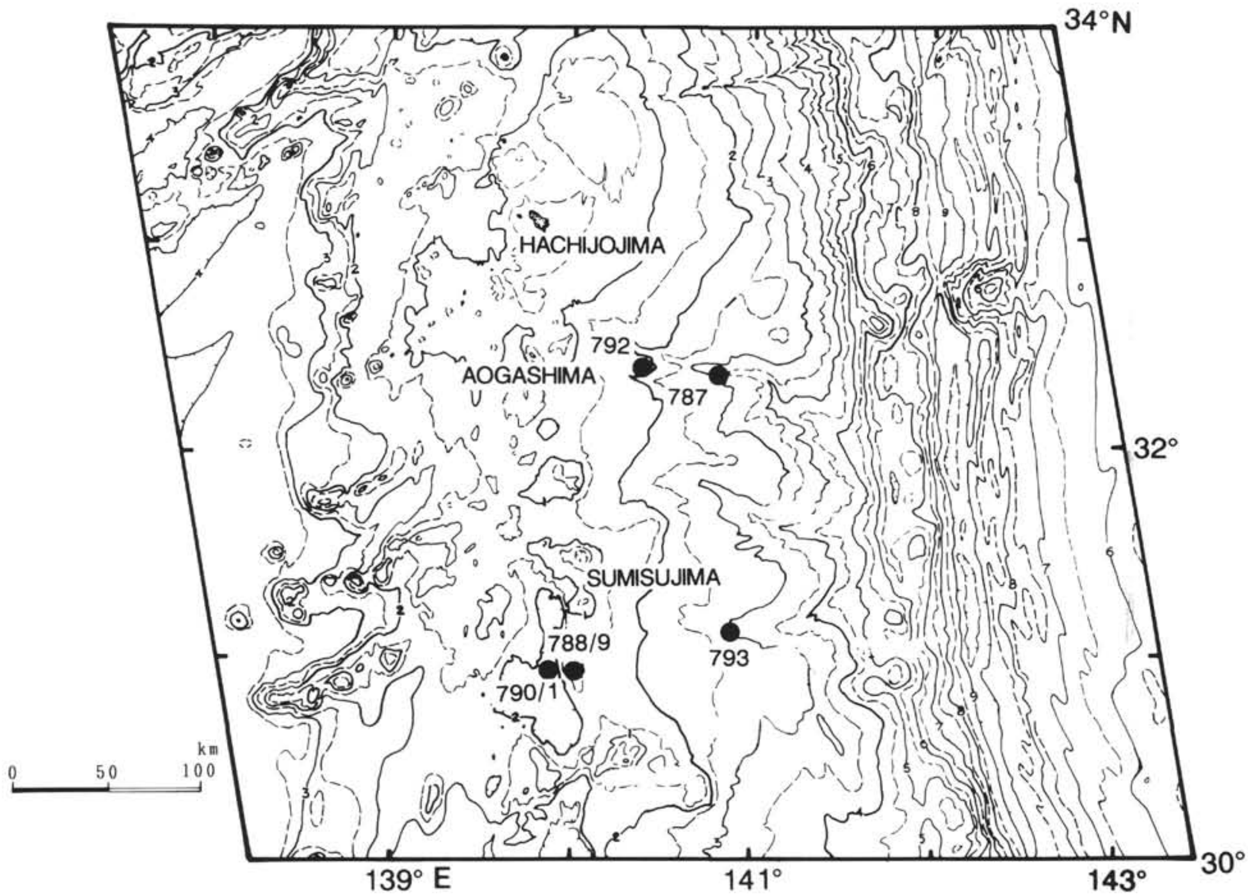

Figure 1. Bathymetric map of the Izu-Bonin Arc-trench system between 30°N and 34°N and locations of the drilling sites (solid circles) of Leg 126. Contour interval = 500 m (numbers on contour lines indicate depth in km).

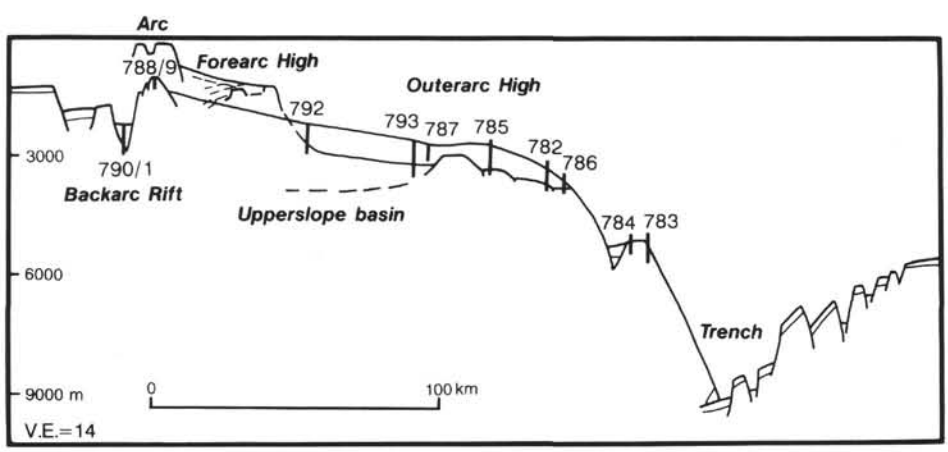

Figure 2. Schematic cross section of the Izu-Bonin Arc with drilling sites. V.E. = vertical exaggeration.

Refractive Indices of Glass

The refractive indices of glass shards from the volcanic ash layers were determined using the automatic refractive index measurements apparatus of Kyoto Fission Track Co. Ltd., Model RIMS-86 following the procedures outlined in Yokoyama et al. (1986). In this procedure, the refraction index value follows the temperature change of the immersion liquid, which is automatically controlled by the instrument's thermomodule. When the glass flakes in the immersion liquid disappear under the microscope, the operator sends a signal to the microcomputer. After the procedural steps are repeated two times (for ascending and descending temperatures) on a glass flake, the micro-

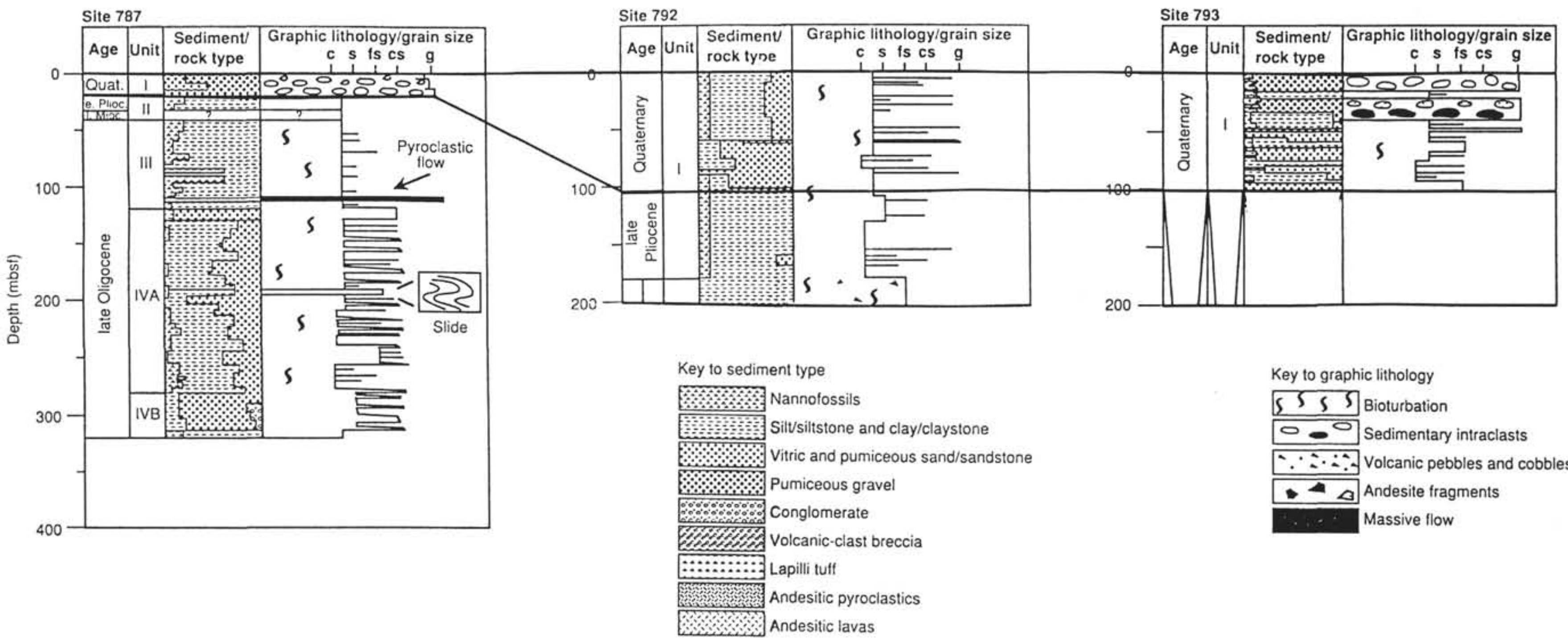

Figure 3. Lithostratigraphic diagram of Izu-Bonin forearc Sites 787, 792, and 793. Solid line indicates the bottom of the Quaternary sediments cored during Leg 126.

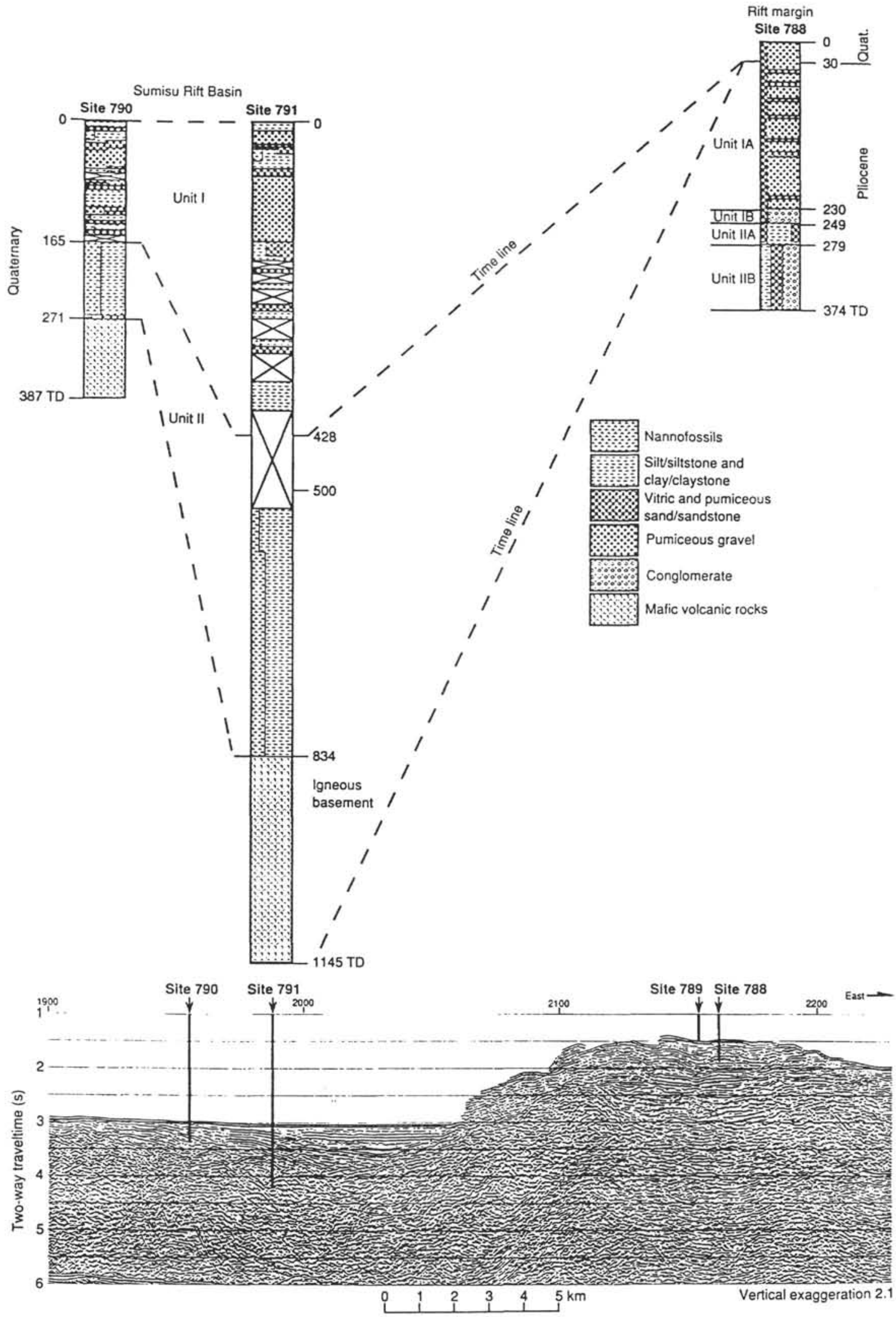

Figure 4. Lithostratigraphic diagram of backarc Sites 790/791 and arc Site 788 (after correlation paper in Taylor, Fujioka, et al., 1990). Upper sketch is the stratigraphic correlation of the backarc sites; lower sketch is the seismic profile of the MCS Line Bon II-4 across the eastern footwall uplift and eastern half-graben of the Sumisu Rift.

computer calculates the mean and standard deviation of the refractive index. The accuracy of the refractive index value of a single glass flake is > 99%.

Chemical Analyses with the Electron Probe Microanalyzer

An electron probe microanalyzer was used to determine the percentage of 12 major elements of the glass shards as well as the minerals in the tephra layers. The tephras were cleaned with an ultrasonic cleaner in distilled water to eliminate clay fractions. Dried samples were impregnated on acrylic plates with 5-mm punches of epoxy resin, and polished thin sections of the volcanic ash layers were prepared. The experimental conditions for analyzing the glass shards were as follows: 15 kV, 1.2×10^{-7} Å, beam diameter of 10 μm, 10-s count for every oxide. Oxides and a single mineral were used as a standard for each oxide. The accuracy of each oxide ranges from 90% to 98%, depending on the element. See Fujioka et al. (1980) and Furuta and Arai (1980a, 1980b) for details of the microprobe procedures.

VISUAL OBSERVATIONS OF VOLCANIC ASH LAYERS

Visual core descriptions and smear slide and binocular observations of the volcanic ash layers were conducted on board the *JOIDES Resolution* and during shore-based studies on the characterization of each ash layer. A list of all the tephras analyzed is given in Table 1. The colors of the tephras are white, gray, green, and black, depending on the chemistry of the glass shards, lithic fragments, and minerals. The glassy tephras are silt-sized, and the scoria and pumice range from sand to granule in size. The thickness of the volcanic ash layers ranges from several tens of centimeters (maximum = 146 cm) to a few millimeters, depending on their distance from the source areas and the degree of bioturbation caused by postdepositional processes. Almost all the tephras are less than 10 cm thick, but tephras several tens of centimeters (60 cm) often occur in turbidites having scoriae and pumices. These thicker layers may be resedimented mixed layers. Sedimentary structures such as laminae, bioturbation, and grading were also observed.

The volcanic glasses recovered during Leg 126 occur as discrete layers and small pods or pockets or are dispersed in the muddy matrices. Some tephra layers have distinct grading structures, some are mixed with rhyolitic and basaltic material, and some are resedimented. Strong burrow structures caused by bottom-dwelling organisms, such as *Zoophycos, Chondrites,* and *Planolites* (Taylor, Fujioka, et al., 1990) also occur in the tephra layers, but these are rare.

Visually, the tephras are classified into two types: simple layer and multiple layer. They also can be classified into mixed and unmixed. The simple layer has a definite boundary in a mud matrix and consists of black and white tephras mixed to form a discrete layer. The multiple layer consists of sets of tephras that have not been diluted by the mud matrices and that have sharp contacts from layer to layer. The existence of the sharp boundaries in the multiple-layer volcanic ash layers suggests that explosive volcanism may take place regularly, with short volcanic quiescent periods intervening in which little or no mud matrix accumulates.

Two types of dark-colored volcanic ash layers were frequently encountered: (1) black, coarse (scoriaceous) and (2) black, fine, well sorted. Two types of light-colored volcanic ash layers were also frequently encountered during visual core observation: (1) white, coarse (pumiceous) and (2) fine, white. These four visually distinct volcanic ashes suggest that their origins are different from each other.

Smear Slide and Binocular Observations

Smear slide descriptions of all the volcanic ash layers sampled are presented in Table 2. Characteristic modes of occurrences of the volcanic glass shards are classified into three major types: translucent, black, and mixed. The translucent type contains more than 85% glass shards with no lithic fragments. The black type has a few lithic fragments and 15%–40% crystals. The mixed type contains both black and translucent volcanic glass shards. The shapes of the volcanic glass shards are bubble wall (bw), tabular (tub), and pumice (pm) for the translucent type and brown-colored, bubble-wall (brbw) and crystal-rich type for the black ashes. Common mineral assemblages for all the volcanic ash layers identified under the petrographic and binocular microscopes are plagioclase, clinopyroxene, and opaque minerals. Orthopyroxene and biotite are rarely encountered. Hornblendes are present but rare in the white ash and crystal-rich black ashes.

ACCUMULATION RATES OF THE VOLCANIC ASH LAYERS

To calculate the accumulation rates of the volcaniclastic materials, we assumed that the input of volcaniclastic material was instantaneous as compared with the hemipelagic muds. Figures 5, 6, and 7 illustrate the accumulation rate of the tephras obtained this way. The accumulation rates of the ash at backarc Sites 790 and 791 show a distinct maximum since 0.2 Ma. The accumulation rate of the volcaniclastic materials of the forearc sites (Figs. 5 and 6) shows two maxima, one around 1.0–0.6 Ma and another at 0.2–0.4 Ma. The older peaks include the rapid accumulation of the dark-colored ashes (i.e., the basaltic ashes). However, the younger peak consisting mostly of rhyolitic ash layers has a much higher accumulation rate. The accumulation rate of the forearc region is quite similar in its pattern to those obtained in the ashes distributed in the south Boso Peninsula (Kotake, 1988).

GRAIN-SIZE DISTRIBUTION OF THE VOLCANIC ASH LAYERS

The grain size of the volcanic ash layers contains information about (1) the origin of the ash, (2) the source region of the tephra, and (3) the depositional mechanism of tephras. The grain-size distribution of the volcanic ash layers of the forearc sites are classified into three types of distribution patterns (Figs. 8A and 8B and Table 3). The first type is characterized by white, coarse ash layers with a median diameter around 3ϕ (Inmann's ϕ scale; Inmann, 1952) and a well-sorted cumulative curve; skewness is small. Examples of this type of grain-size distribution include Samples 126-792A-4H-4, 96–98 cm, and 126-792B-19H-2, 36–38 cm. The second characteristic distribution is a black ash that has a well-sorted cumulative curve with a 3–4ϕ median diameter; skewness is small, but kurtosis is high. Examples of this type of grain-size distribution include Samples 126-792A-3H-5, 78–80 cm, and 126-793A-3H-2, 50–52 cm. The third characteristic grain-size distribution is typified by a fine white ash layer, either well or poorly sorted, with a median diameter of 4ϕ. The poorly sorted tephras are skewed toward the finer portions, whereas skewness is small in the well-sorted portion. Examples of the third grain-size distribution type include Samples 126-788C-11H-4, 108–110 cm, 126-792A-1H-5, 81–83 cm, and 126-793A-3H-2, 69–71 cm. Tephras with well-sorted, fine median diameters may be the result of fallout deposits, whereas those skewed toward a finer grain size may be the result of subaqueous volcanism (Sparks et al., 1981; Walker, 1971).

The tephra grain-size distribution suggests that distribution types 1 and 2 represent input from a nearby source (i.e., the Izu-Bonin Arc), but the black tephras with low kurtosis may come from secondary processes. The third type of tephra grain-size distribution may represent input from the western part of the Philippine Sea.

The backarc tephras are classified into two types of grain-size distribution curves: coarse pumiceous and fine glass. Characteristic features of the coarse tephras include a broad size distribution ranging from clay to granule size (Nishimura et al., this volume); medium

Table 1. Volcanic ash layers at Site 790.

Layer no.	Core, section, interval (cm)	Thickness (cm)	Description and remarks
Hole 790B			
1	1H-1, 14(top)–140(base)	726	Thick pumice layer
	2H-2		
2	2H-2, 145–150*	5/3/2	Very dark gray(5Y3/1)/brownish black(5YR2/1/grayish black(N2); silt/silt/v.f.sand
	2H-3,*0–5		
3	2H-3, 7–11	4	Brownish black(5YR2/1); silt
4	2H-3, 17–20	3	Brownish black(5YR2/1); silt
5	2H-3, 39–46	7	Grayish black(N2)/brownish black(5YR2/1); silt
6	2H-3, 148–150*	20	Grayish black(N2); silt (laminated at lowest 5 cm)
	2H-4, *0–18		
7	2H-4, 61–74	3	Light olive gray(5Y6/1); silt
8	2H-4, 127–150*	76/85	Light olive gray(5Y4/1); silt/v.f.s-m.s(grading)
	2H-5, *0–138		
9	2H-6, 42–77	35	Brownish black(5YR2/1); silt
10	3H-1, 27–56	29	Grayish black(N2); silt
11	3H-1, 70–150*	44/65	Grayish black(N2); silt/f.-m.sand(laminated)
	3H-2, *0–29		
12	3H-2, 58–150*	152/77	Olive gray(5Y5/2)/olive gray(5Y4/2)/dark olive gray(5Y3/2); silt/silt-m.sand(grading)
	3H-3,*0–137		
13	3H-4, 29(top)–7(base)	3628	Thick pumice layer II
	7H-3		
14	7H-3, 27–31	4	Brownish black(5YR2/1); silt
15	7H-3, 63–66	3	Olive black(5Y2/1); silt
16	7H-3, 85–93	3/3/2	Olive gray(5Y4/1)/olive gray(5Y4/1); silt/silt/silt
17	7H-3, 115–150*	50/55/	Gray(5Y5/1)/olive gray(5Y4/2)olive gray(5Y4/1)/(5Y4/1)/olive gray(5Y4/2)/(5Y4/2)/(5Y4/2); silt/silt/v.f.sand/v.f.sand/f.sand
	7H-4, *0–150**	230/45/	
	7H-5, **0–150***	35/50	
	7H-6, ***0–130		
18	7H-6, 143–147	4	Reddish gray(10R6/1); silt
19	8H-1, +0–150*+	90/25/11	Light gray(5Y7/1)/gray(5Y5/1)/(5Y5/1)/olive gray(5Y4/1)/(5Y5/1)/(5Y4/1)dark olive gray(5Y3/2)/olive black(5Y2/1); pumice granule (maximum diameter=3.5 cm)/mixture of pumice pebble and silt/silt/silt/silt/silt/v.f.sand/f.sand
	8H2, *0–90	/1/23/70/17/3	
20	8H-2, 106–150*	39/1/40	Brownish black(5YR2/1)/grayish black(N2)/olive black(5Y2/1)/(N2)/(N2)/dark olive gray(5Y3/2); silt/v.f.sand/silt with grayish black v.f.sand thin layers/v.f.sand/f.sand/v.f.sand
	8H-3, *0–85	/9/32/8	
21	8H-3, 143–148	5	Dark olive gray(5Y3/2);v.f.sand
22	8H-4, 0–38	35/3	Olive black(5Y2/1); silt/f.sand(laminated)
23	8H4, 48–62	10/2/2	Olive black(5Y2/1)/grayish black(N2)/olive black(5Y2/1); silt/v.f.sand/silt
24	8H-4, 115–150*	26/18	Olive black(5Y2/1)/grayish black(N2); silt with v.f.sand laminated/v.f.-f.sand(grading)
	8H-5, *0–9		
25	8H-5, 38–131	11/41/41	Brownish black(5YR2/1)/olive black(5Y2/1)/grayish black(N2); f.sand with pumice m.sand laminated/silt with grayish black(N2) v.f.sand thin layers/v.f.-m.sand(grading)
26	8H-6, 14–17	3	Dark olive gray(5Y3/2); silt
27	8H-6, 33–35	2	Dark olive gray(5Y3/2); silt
28	8H-6, 54–63	9	Gray(5Y5/1); silt
29	8H-6, 74–92	3/2/7/2/2	Olive black(5Y2/1)/grayish black(N2)/olive black(5Y2/1)/grayish black(N2)/olive black(5Y2/1); silt/v.f.sand/silt/v.f.sand/silt
30	8H-7, 43(top)–15(base)	1622	Thick pumice layer III
	10H-5,		
31	10H-5, 22–24	2	Brownish black(5YR2/1); silt
32	10H-5, 32–150*		Olive gray(5Y4/1)/dark greenish gray(5GY4/1)/(5Y4/1)/very dark gray(5Y3/1)/(5Y4/1)/(5Y4/1)/olive gray(5Y4/2)/(5Y4/1)/(5Y4/2)/(5Y4/1)/(5Y4/2)/dark olive gray(5Y3/2)/(5Y3/2)/gray(5Y5/1)/olive black(5Y2/1)/(5Y3/2); silty clay/silty clay/silt/silt/silt/v.f.sand/silty v.f. sand/silt/v.f.sand/silt/c.silt/v.f.sand/f.sand/f.sand/m.sand
	10H-6,*0–146	5/5/83/2/23/8/ 1/4/5/6/4 4/34/14/2 /8/20	
Hole 790C-			
33	1H-4, 70–72	2	Olive gray(5Y4/1); v.f.sand
34	1H-4, 115(top)–43(base)	3628	Thick pumice layer IV
	5H-3		
35	5H-3, 55–59	4	Olive(5Y5/4); f.sand
36	5H-3, 67–70	3	Olive(5Y5/4); f.sand
37	5H-3, 87	<1	Dusky green(5G3/2); silt
38	5H-3, 91–111	20	Grayish black(N2); clayey silt-f.s(grading)
39	5H-3, 111–150*	39/60	Grayish black(N2)/dark gray(N3); silt/c.sand(grading)
	5H-4, *0–60		
40	5H-4, 96–136	26/14	Dark gray(N3)/black(N1); clayey silt/m.sand
41	5H-5, 6–15	9	Dark gray(N3); silt
42	5H-5, 20–35	15	Dark gray(N3);clayey silt/v.f.sand
43	5H-5, 43–95	49/3	Dark gray(N3)/grayish black(N2); clayey silt/m.sand
44	5H-6, 6–21	15	Medium dark gray(N4); silt-v.f.sand(grading)
45	5H-6, 62–72	10	Medium dark gray(N4); silt-v.f.sand(grading)
46	5H-6, 82	<1	Dusky green(5G3/2); silt
47	5H-6, 85	<1	Dusky green(5G2/1); silt
48	5H-6, 120–150	++2/28+	Medium light gray(N6)/olive gray(5Y4/1); silt/silt
49	6H-1, +0–150*	++150/31	Olive gray(5Y4/1)/olive gray(5Y4/1); f.-m.sand/pumiceous m.-c.sand(grading)(laminated)
	6H-2, *0–31		
50	6H-2, 47–65	18	Light olive gray(5Y6/1); f.sand(grading)
51	6H-2, 80–144	57/7	Light olive gray(5Y6/1)dark gray(N3); silty clay/m.sand
52	6H-3, 34–135	29/73	Light olive gray(5Y6/1)/medium gray(N5); silt/m.sand(grading) (pumice maximum diameter=1 mm)
53	6H-4, 5–51	5/25/16	Light olive gray(5Y6/1)/light olive gray(5Y6/1)/dark gray(N3); f.s/silty clay/m.sand

Table 1 (continued).

Layer no.	Core, section, interval (cm)	Thickness (cm)	Description and remarks
54	6H-4, 60–81	11/10	Light olive gray(5Y6/1)/dark gray(N3); silty clay with scattered pumice/f.sand with an erosive base
55	6H-4, 99–140	2/23/16	Olive gray(5Y4/1)olive gray(5Y4/1)/dark gray(N3); silty v.f.sand/silty clay/m.sand
56	6H-5, 7–77	52/18	Light olive gray(5Y6/1)/dark gray(N3); clayey silt/f.sand (laminated)
57	6H-5, 96–118	14/8	Light olive gray(5Y6/1)/dark gray(N3); clayey silt/f.sand (laminated)
58	6H-5, 141–150* 6H-6, *0–37	29/17	Light olive gray(5Y6/1)/dark gray(N3); clayey silt/silty v.f.sand
59	6H-6, 41–47	6	Light olive gray(5Y6/1): v.f.sand
60	6H-6, 73–142	11/53/5	Light olive gray(5Y6/1)/light olive gray(5Y6/1)/dark gray(N3); silty clay/silty f.sand/f.sand
61	7H-1, +0(top)–18(base) 8H-CC,	++1250+	Thick pumice layer V
62	11X-1, 25	<1	Silt
63	11X-2, 10–16	6	Very light gray(N8); clayey silt-v.f.sand(grading)
64	11X-2, 45–50	5	(10Y6/2); silt(grading)
65	11X-3, 17–30	12/1	Olive gray(5Y5/2)/very light gray(N8); clayey silt-v.f.sand(grading)/clayey silt
66	11X-3, 109–110	1	Very light gray(N8); silt
67	11X-4, 32–47	10/5	Olive gray(5Y5/2)/dark gray(N3); clayey silt/c.sand
68	11X-4, 70–72	2	Medium light gray(N6); v.f.sand
69	11X-4, 110–120	10	Dark gray(N3); silt(grading)
70	11X-4, 139–150*	15/4/3/3	Olive gray(5Y5/2)/olive gray (5Y5/2#/light gray(N7)/medium dark gray(N4); silt/m.sand/silt/v.f.sand with and erosive base
71	12X-1, 5–14	9	Olive gray(5Y4/1); silt
72	12X-1, 20–23	3	Olive gray(5Y4/1); silt
73	12X-1, 26–28	2	Olive gray(5Y4/1); silt
74	12X-1, 35–37	2	Olive gray(5Y4/1); silt
75	12X-1, 40–42	2	Olive gray(5Y4/1); silt
76	12X-1, 45–69	5/4/6/4/5	Olive gray(5Y4/2)/olive gray(5Y4/1)/olive gray(5Y4/2)/olive black(5Y2/1)/olive black(5Y2/1); silt/silt/m.sand with pumice c.sand/f.sand/silt
77	12X-1, 71–76	5	Olive black(5Y2/1); f.sand
78	12X-1, 130–140* 12X-CC, *0–33	43+	Light olive gray(5Y4/1); silt
79	13X-1, 18–44	7/5/4	Gray(5Y5/1)/olive gray(5Y4/1)/olive black(5Y2/1); clayey silt/silt/f.sand
80	13X-1, 50–52	2	Olive gray(5Y4/2); silt
81	13X-1, 66–68	2	Olive black(5Y2/1); silt
82	13X-1, 71–72	1	Olive black(5Y2/1); silt
83	13X-1, 79	<1	Olive black(5Y2/1); silt
84	13X-1, 81	<1	Olive black(5Y2/1); silt
85	13X-2, 15–55	31/9	Gray(5Y5/1)/gray(5Y5/1); clayey silt/silt
86	13X-3, 71–75	4	Gray(5Y5/1); silt
87	14X-1, +0–7	++7	Gray(5Y5/1); silt
88	14X-1, 87–88	1	Light brownish gray(5YR6/1); clayey silt
89	14X-1, 136–147	6/5	Very dark gray(N2)/olive gray(5Y4/1); f.sand/scoria granule (maximum diameter= 1cm)
90	15X-1, 7–8	1	Olive black(5Y2/1); silty v.f.sand
91	15X-1, 12–17* 15X-CC, *0–5	10	Olive black(5Y2/1); m.sand
92	15X-CC, 10–22+	12+	Olive black(5Y2/1); m.sand
93	16X-1, +0–28	++7/3/16/2	Gray(5Y5/1)/very dark gray(5Y3/1)/gray(5Y5/1)/very dark gray(5Y3/1); silt/silt/silt/v.f.sand
94	16X-1, 99–104	5	Olive gray(5Y4/1); silt
95	16X-1, 106	<1	Olive gray(5Y4/1); silt(5 mm thick)
96	16X-2, 8–12	4	Olive gray(5Y5/2); silt
97	16X-2, 35–38	3	Gray(5Y5/1); silt
98	16X-4, 63–67	1/3	Dark olive gray(5Y3/2)/olive gray(5Y4/1); silt
99	16X-5, 52–66	14	Very dark gray(5Y3/1); m.sand
100	16X-5, 118–120	2	Light olive gray(5Y6/1); silt
101	16X-6, 17–20	3	Olive gray(5Y4/2); silt
102	16X-CC, 0–4	4	Dark olive gray(5Y3/2); silt
103	16X-CC, 18–20	1/1	Gray(5Y5/1)/dark olive gray(5Y3/2); silt
104	17X-1, 130–145	15	Olive gray(5Y4/1); silt-sandy silt(grading)
105	17X-7, 27–32	2/2/1	Very dark gray(5Y3/1)/olive gray(5Y4/2)/olive black(5Y2/1); silt/silt/m.sand
106	17X-CC, 34–35	1	Light olive gray(5Y6/1); silt
107	18X-1, 145	<1	Silt
108	18X-3 135–136	1	Silt
109	18X-4, 58–60	2	Very light gray(N8); silt
110	18X-4, 100	<1	Very light gray(N8); silt
111	18X-4, 123–124	1	Very light gray(N8); silt
112	19X-1, 46–53	7	Olive gray(5Y4/2) silt
113	19X-1, 65–68	3	Olive gray(5Y4/2) silt
114	19X-1, 94–96	2	Gray(5Y5/1); silt
115	19X-2, 98–106	8	Gray(5Y5/1); silt
116	19X-3, 52–60	8	Olive gray(5Y4/2); clayey silt
117	19X-3, 81–85	4	Olive gray(5Y4/2); clayey silt
118	19X-4, 92–150* 19X-5, *0–3	36/14/11	Dark gray(N3)/grayish black(N2)/olive black(5Y2/1); pebble-granule gravel with sandy silt
119	19X-5, 57–59	2	Olive gray(5Y4/2); silt
120	19X-6, 13–14	1	Medium light gray(N6); silt
121	19X-6, 20	1	Medium light gray(N6); silt pocket
122	19X-6, 39–45	4/2	Olive gray(5Y5/2)/light olive gray(5Y6/1); silt
123	20X-2, 63–150*	217	Pumice gravel scattered in sandy mud (maximum diameter=4 cm)
124	20X-CC, 28–50+	6/16+	Light olive gray(5Y6/1)/grayish black(N2); sand/scoria (maximum diameter=2 cm)

Note: Sample 126-790B-10H-6, 140 cm, is correlative to 126-790C-1H-4, 57 cm. v.f. = very fine, v.f.s. = very fine sand, m.s. = medium sand, f. = fine, m. = medium, and c = coarse. The list for forearc Site 792 is given in Fujioka et al. (this volume).

*Continue to the next * below.

+Continue to the next + or ++ below.

Table 2. Petrographic characteristics of backarc tephras at Sites 790/791.

Core, section, Interval (cm)	Lithology	Thickness (cm)	Grain size	Max gl (mm)	Max li (mm)		Mode (gl%/cry%/li%)	Constituent minerals						Glass shape	Refractive Index			Comment	
								pl	cpx	opx	hb	bi	op		(mean)	(min)	(max)		
126-790A-																			
1H-1, 139-141															1.5085	1.5067	1.5106		
1H-3, 52-54															1.5087	1.5063	1.5102		
1H-6, 49-51																			
2H-1, 96-98																			
2H-2, 24-26															1.5152	1.5125	1.5172		
2H-4, 139-141																			
2H-5, 148-150																			
2H-7, 30-32															1.5111	1.5047	1.5131		
3H-1, 66-68																			
3H-3, 40-42																			
4H-3, 83-85																			
4H-5, 30-32																			
2H-3, 9-11																			
2H-3, 26-28																			
2H-4, 63-65																			
2H-6, 68-70																			
4H-2, 24-26																			
4H-6, 139-141																			
5H-1, 142-143																			
5H-4, 133-135																			
6H-4, 31-33																			
7H-2, 129-131																			
7H-6, 146-147			v.f.sand- f.sand	0.3			92/ 8/0	++	++	++				pum,br				br mixed	
8H-3, 8-10																			
8H-4, 34-36																			
8H-4, 60-64																			
8H-5, 7-9																			
8H-5, 46-48																			
8H-6, 84-86																			
10H-4, 130-132																			
10H-6, 123-125																			
11H-6, 100-102																			
15X-1, 58-60																			
126-790C-																			
1H-2, 133-135			v.f.sand- m.sand	0.3	0.1		80/10/10	++					++	pum,bw					
2H-6, 128-130																			
3H-1, 110-112			v.f.sand	0.12			93/ 7/0	++			++			bw					
3H-5, 10-12			v.f.sand- f.sand	0.2			88/12/0	++						bw					
3H-6, 44-46			v.f.sand- f.sand	0.25			90/10/0	++						bw					
4H-1, 113-115																			
4H-2, 59-61																			
4H-3, 21-23																			
4H-4, 65-67			f.sand - c.sand	0.2	0.25		60/60/10	++	++		++		++					crystal(Max 0.5mm)	

Table 2 (continued).

Core, section, interval (cm)	Lithology	Thickness (cm)	Grain size	Max gl (mm)	Max li (mm)		Mode (gl%/cry%/li%)	Constituent minerals pl	cpx	opx	hb	bi	op	Glass shape	Refractive Index (mean)	(min)	(max)	Comment	
4H-5, 97-99																			
4H-6, 33-35																			
5H-1, 79-81																			
5H-3, 72-74																			
5H-5, 4-6			v.f.sand- m.sand	0.4	0.2		90/ 7/3	++	++	+	++		+	bw				br glass mixed	
5H-5, 104-106																			
5H-6, 116-118			v.f.sand	0.15			90/10/0	++					++	bw				op rich	
6H-2, 51-53			v.f.sand	0.15			90/10/0	++					++	bw					
6H-2, 139-141																			
6H-3, 80-82			f.sand - m.sand	0.4			95/ 5/0	++			++			bw					
6H-4, 27-29			v.f.sand- f.sand	0.15	0.05		88/10/2	++	++	++	+		+	bw>cry					
6H-4, 78-80																			
6H-5, 21-23																			
6H-6, 10-12			v.f.sand- m.sand	0.45	0.1		80/12/8	++	++		++			bw>br					muddy
6H-6, 92-94			v.f.sand- m.sand	0.35	0.15		89/10/1	++			++			bw>pum					muddy
7C-4, 44-46			v.f.sand- f.sand	0.25	0.3		93/ 6/1	++					++	bw					muddy
8C-4, 140-142																			
8H-6, 140-142																			
10X-1, 50-52																			
11X-2, 10-12			v.f.sand	0.2			95/ 5/0	++	++		++		+	bw				very fine	
11X-3, 110-112			f.sand	0.2	0.15			++		+	++			pum,tub					muddy
11X-4, 50-52																			
11X-4, 76-78			v.f.sand	0.1	0.05		65/30/5	++			+			bw					
12X-1, 21-23			f.sand - m.sand	0.4	0.15		85/10/5	++			++			pum,tub					muddy
12X-1, 65-67																			
13X-1, 41-43																			
13X-2, 64-65																			
14X-2, 135-137																			
16X-1, 9-11																			
16X-5, 63-65																			
17X-7, 29-31																			
18X-4, 121-123																			
19X-1, 94-96			v.f.sand- f.sand	0.2			95/ 5/0	++			+		++	pum					muddy
19X-4, 137-139																			
19X-6, 77-79																			
20X-3, 109-111																			
20X-5, 20-22																			
126-791A-																			
2H-5, 74-76			v.f.sand- f.sand	0.25	0.1		87/10/3	++			++		++	bw	1.508	1.5051	1.5105	br,pum,li mixed	
3H-1, 92-94			v.f.sand- m.sand	0.4	0.15		90/ 8/2	++			++		++	bw				br glass mixed	
4H-4, 104-106																			
4H-5, 99-101															1.5087	1.5075	1.5097		
5H-2, 142-144																			
5H-3, 78-80																			
5H-4, 16-18																			

Table 2 (continued).

Core, section, interval (cm)	Lithology	Thickness (cm)	Grain size	Max gl (mm)	Max li (mm)		Mode (gl%/cry%/li%)	Constituent minerals pl	cpx	opx	hb	bi	op	Glass shape	Refractive Index (mean)	(min)	(max)	Comment	
6H-2, 60-62															1.5054	1.5023	1.5091		
7H-2, 80-82			v.f.sand- f.sand	0.2			96/ 4/0	++					++	bw	1.507	1.5053	1.5097		
8H-7, 29-31																			
9H-6, 134-136																			
10H-5, 117-119																			
12H-3, 102-104																			
14H-4, 35-37																			
15H-1, 130-131																			
15H-4, 121-122																			
16H-1, 48-51																			
17H-2, 110-111																			
17H-6, 20-21																			
18H-1, 5-7			v.f.sand	0.15	0.05		80/15/5	++	+				++	bw					muddy
18H-1, 53-55			v.f.sand	0.1	0.05		80/20/5	++	+		+		++	bw					
19H-1, 45-47			v.f.sand- m.sand	0.3			98/ 2/0	++						bw					muddy
19H-6, 132-134			v.f.sand- f.sand	0.25	0.15			++			+			bw				Max crystal 0.35mm	
20H-1, 2-4																			
20H-2, 91-93																			
21H-1, 22-24																			
22H-6, 78-80																			
22H-6, 110-112																			
23H-2, 98-100																			
25X-2, 20-22																			
28X-1, 25-27																			
30X-CC (18-20)																			
33X-1, 50-52																			
39X-1, 90-92			v.f.sand- m.sand	0.3	0.25		94/ 5/1	++					++	bw>pum	1.5126	1.509	1.5133		
42X-1, 31-33			v.f.sand- f.sand	0.3	0.2		95/ 5/0	++					++	bw	1.5072	1.5057	1.5101		

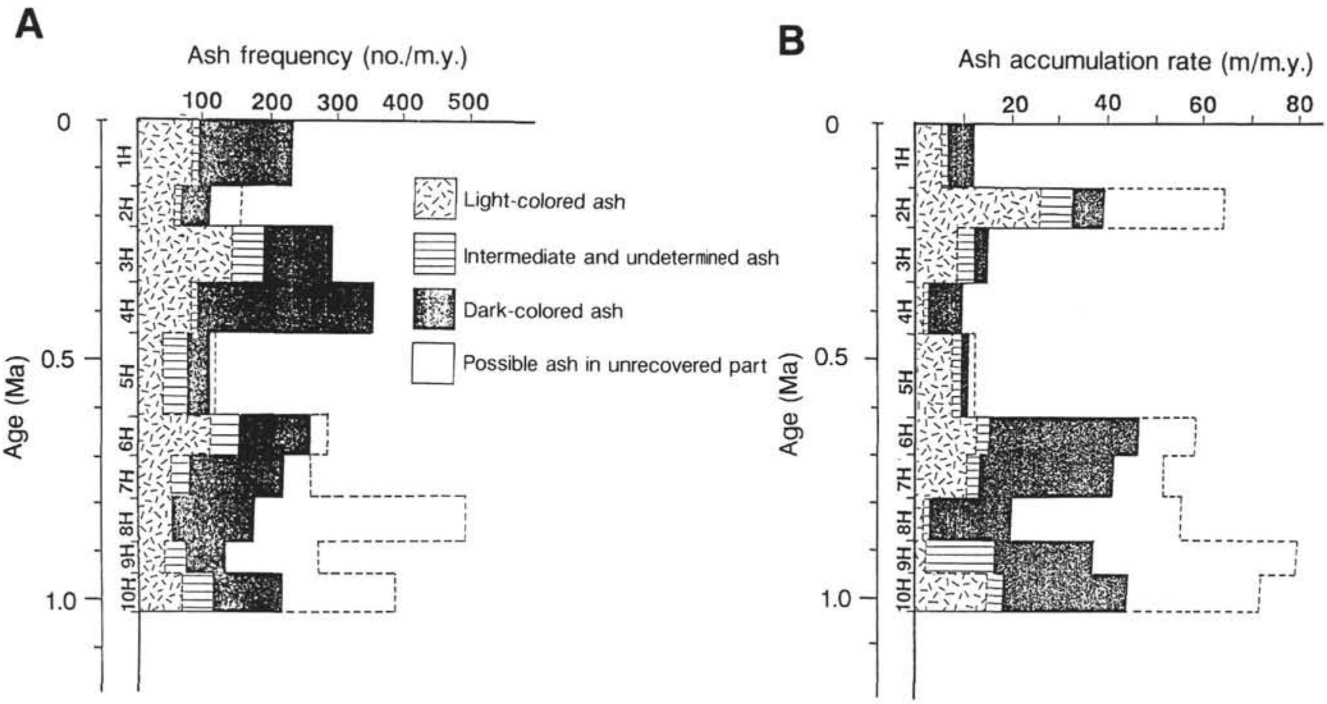

Figure 5. Accumulation rate of the Quaternary volcaniclastic materials of forearc Site 792. **A.** Ash frequency indicated by ash number per million years, calculated by the constant sedimentation rates of muddy hemipelagites. **B.** Ash sedimentation rate obtained by the same method as in A.

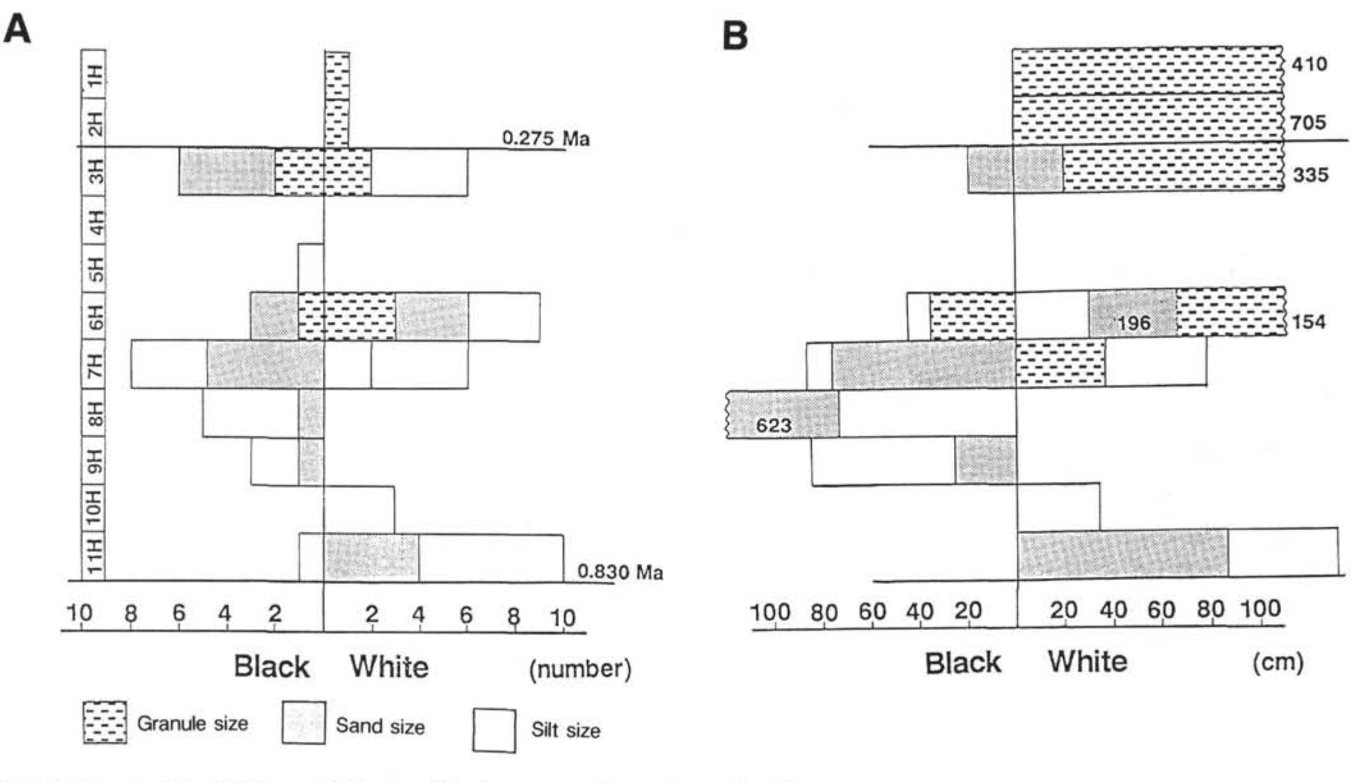

Figure 6. Frequency (**A**) and thickness (**B**) diagram of the Quaternary tephras at forearc Site 793.

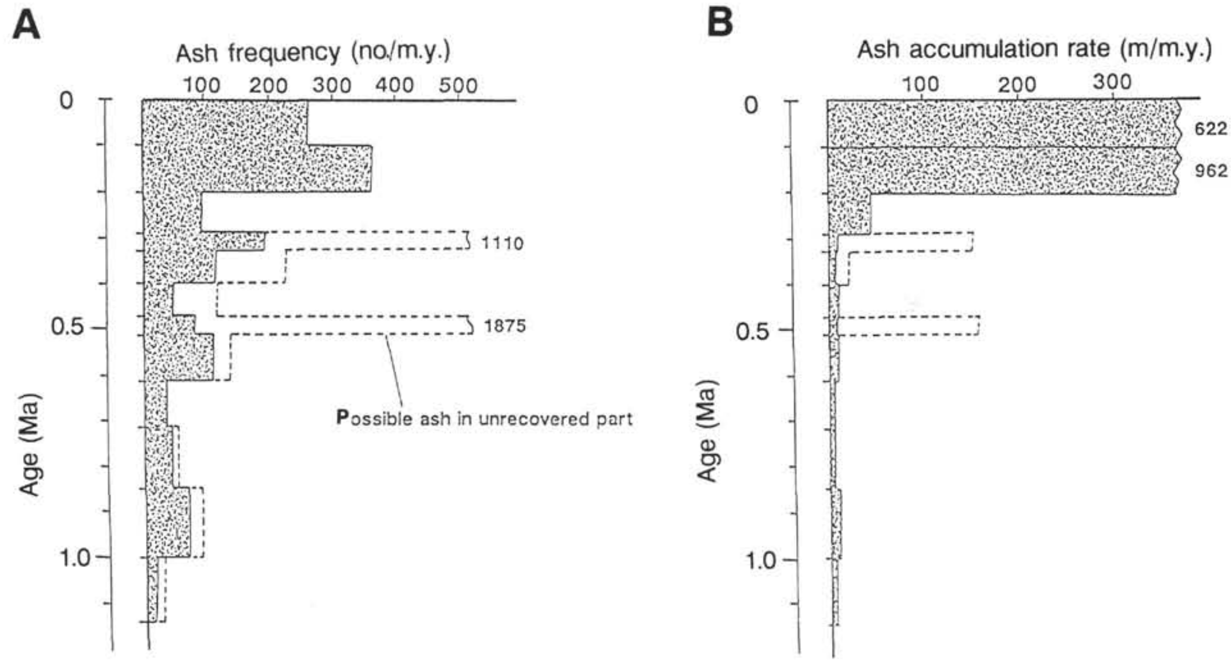

Figure 7. Frequency (**A**) and accumulation (**B**) diagram of the tephras at backarc Sites 790/791.

diameters of the pumice fragments range from 200 to 600 µm. Examples of this type include Samples 126-791A-22H-6, 28–32 cm, and 126-791A-4H-3, 6–10 cm (Fig. 9). This type of grain-size distribution represents resedimented deposits (Sparks et al., 1981; Taylor, Fujioka, et al., 1990). In contrast, the fine glassy tephras have a well-sorted distribution curve, with median diameters ranging from 60 to 100 µm. Examples of this type include Samples 126-790B-7H-6, 146–147 cm, and 126-790C-7H-4, 44–46 cm (Fig. 9). Fine glassy ashes are often associated with coarse thick pumiceous tephras, suggesting they originate from a subaqueous eruption (Fisher, 1984; Kokelaar et al., 1985; Fiske, 1986; Fiske and Cashman, 1989).

CHEMISTRY OF THE VOLCANIC GLASS SHARDS

Tephras from Leg 126 sites belong to the low-alkali tholeiitic series on Kuno's silica-alkali diagram (Figs. 10–12; Kuno, 1966). Generally, tephras at Site 788 are slightly different from those at the backarc and forearc sites in several respects. First, the tephras at Site 788 have very low SiO_2, Na_2O, and K_2O concentrations (Table 4). Second, at the forearc and backarc sites, tephras extremely enriched in K_2O were recognized in some intervals. Sometimes K_2O contents exceeded 4 wt%. These kinds of tephras may possibly come from the western regions, as discussed below.

The total alkali content of Site 788 tephras is quite constant, that is, Na_2O and K_2O change sympathetically with time. The total alkali contents of Site 790 tephras vary only slightly, but the youngest ones are quite low in K_2O, Na_2O, and total alkali. Tephras at Sites 792 and 793, however, vary greatly over time. See Appendix (on microfiche in back pocket) for the chemical composition data of the volcanic glasses at arc Site 788 and backarc Sites 790/791.

CORRELATION OF THE ASH LAYERS

Establishing a correlation of the volcanic ash layers is necessary to determine the volcanic history in the Izu-Bonin areas as well as in other regions around the Japanese Islands. Although most of the 300 tephras identified in this study have different but similar chemical and mineralogical compositions, several have quite distinct characteristics that are comparable to tephras identified in other studies. Here we show four examples of correlations of tephras from the Izu-Bonin forearc to the other sites and volcanic islands. The distinctive properties of these volcanic ash layers are listed in Table 5.

Samples 126-792A-3H-1, 80–94 cm, and 126-793A-4H-2, 96–98 cm

These tephras have similar refractive indices and chemical compositions as well as glass shard types and mineral assemblages. Their age is estimated to be equivalent to Zone CN14b.

Samples 126-792A-5H-3, 131–133 cm, and 442A-5-3, 30–34 cm

These two ash layers have similar refractive indices and chemical compositions as well as similar glass shard types and mineral assemblages. Therefore, these two ashes may be correlative with each other although they are several hundred kilometers apart. The origin of this tephra may be further west of the Shikoku Basin, for example, from the Ryukyu Arc.

Black Tephras at Site 792 and Aogashima Volcanics

The chemical compositions of the Kurosaki volcanics, in the lowermost sequence of Aogashima Island, have distinctly different chemical characteristics as compared with younger sequences, that is, low TiO_2 and K_2O contents and high FeO and CaO contents (Takada et al., in press). The chemical compositions of some black volcanic ash layers at Site 792 are quite similar to those of the Kurosaki volcanics. Examples include Samples 126-792A-4H-1, 117–119 cm, and 126-792A-4H-3, 20–22 cm.

Samples 126-792A-1H-5, 81–83 cm, and Aso-4

The white coarse volcanic ash layer at Hole 792A has quite similar mineral assemblages, refractive indices, and chemical compositions as well as ages and glass shard shapes to that of Aso-4 (Furuta et al., 1986) of the Aso Volcano, Kyushu. The type of glass shard in the

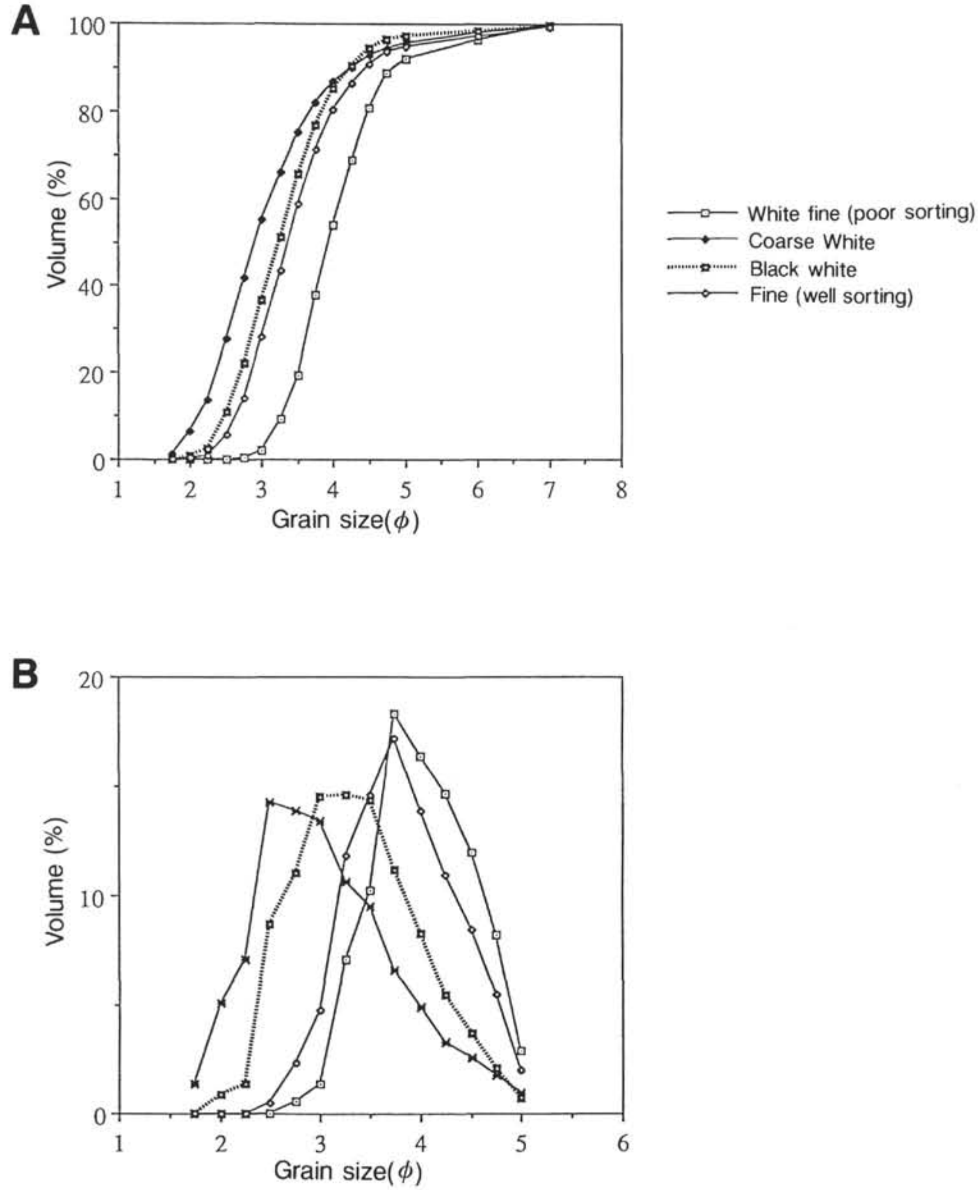

Figure 8. Grain-size characteristics of four types of tephras. **A.** Cumulative frequency grain-size curve for all the tephras at Site 792, Izu-Bonin forearc. **B.** Frequency grain-size distribution curve for volcanic ash layers at Site 792. Scale of the grain size is represented by ϕ (phi).

Aso-4 is bubble wall with a pale brown color. The age of this tephra is estimated to be 70–80 ka according to stratigraphic data obtained on land (Machida and Arai, 1983) and around 80 ka according to U-Th age determinations (Omura, 1984).

DISCUSSION

The chemical characteristics of the tephras from the Pliocene-Pleistocene ages have low K_2O contents similar to the keratophyre of the Paleozoic rift as well as low-K rhyolite in the rift area (Gill, 1981; Gill et al., 1984; Reagan and Meijer, 1984; Hawkins and Melchior, 1985; Brouxel et al., 1987; Hochstaedter et al., 1990a, 1990b).

Volcanism in this stage shows the characteristic basaltic and rhyolitic bimodal distribution in both chemical and visual compositions. This kind of bimodal volcanism was noted in the basin and range province of the Cascade region of the North America, where extensional stress fields predominated from Eocene to Holocene times (Christiansen and Lipman, 1972; Eaton, 1982, 1984). Kennett et al. (1979) noted the characteristic volcanic pulse of the Quaternary period in the circum-Pacific regions and named this pulse "Cascadian." The Izu-Bonin explosive volcanism is also similar in character to the Cascadian event.

The numbers of Pliocene-Pleistocene volcanic ash layers increased in this area, and thick tephra piles accumulated (Fujioka et al., this volume). From the grain-size distribution and chemical compositions, we determined that the tephras came mostly from along the present Izu-Bonin Arc, although some tephras possibly came from a more western part of the Philippine Sea (i.e., from the Ryukyu Arc).

Along the Ryukyu Arc, the late Miocene to Pliocene Shimajiri Group yielded many coarse tephras including pumices (Konishi,

Table 3. Grain-size analyses data for Sites 788, 790, and 791.

Site		788C	788C	790A	790A	790A	790A	790A	790A	790A	790B	790B
Core, section		11H-3	11H-4	1H-1	1H-3	2H-1	2H-2	2H-4	2H-5	3H-1	2H-3	2H-3
Interval (cm)		38-40	108-110	139-141	52-54	96-98	24-26	139-141	148-150	66-68	11-Sep	26-28
Cumulative volume percentages	Class interval (ϕ)											
	1.75-	0	0	0	0	0	0	0	0	2	0	0
	2.00-1.75	0	1.2	0	0	0	0	0.7	0	8.4	0	0
	2.25-2.00	0.1	3.1	0	0	0	0	1.8	0	17.3	0	0
	2.50-2.25	3.3	14	0	1.3	0.5	1.8	9.4	0.2	17.3	0	0
	2.75-2.50	11.1	26.9	0.5	5.3	3.1	6.9	20.5	1.8	31.7	0.9	0.8
	3.00-2.75	25.5	42.8	1.8	13.3	8.8	16.8	36.7	5.4	45.1	3.1	2.8
	3.25-3.00	41.8	57.2	8.6	27	24.1	30.9	52.8	17.2	57.3	12.9	11.5
	3.50-3.25	58.5	70.7	18.3	42.7	42.8	46.3	68.4	32.1	66.6	26.1	23.1
	3.75-3.50	71.7	79.7	35.2	58.7	62.6	60.8	79	49.2	74.9	45.1	39.2
	4.00-3.75	81.3	86	50.6	71.2	77.5	72.1	86.4	63.1	80.9	61.3	53
	4.25-4.00	87.6	89.7	64.6	80.5	87.8	80.4	90.9	73.9	85.6	74.9	64.7
	4.50-4.25	92	92.3	76.8	87.5	94.3	86.8	94	82.2	89.1	85.3	74.3
	4.75-4.50	94.7	93.9	85.7	92.1	97.7	91.1	95.8	87.7	91.9	92.1	81.1
	5.00-4.75	95.6	94.6	89.7	93.8	98.2	92.8	96.4	89.6	92.7	94.3	84
	5.00-6.00	97.3	97	95.6	96.6	99.1	96.2	98	93.6	95	97.7	91.2
	7.00-6.00	99.3	99.1	99.4	99.4	99.8	99.3	99.6	98.2	97.2	99.8	97.7

Site		790B	790B	790B	790B	790B	790B	790B	790B	790B	790B	790B	790B
Core, section		2H-4	2H-6	4H-2	4H-6	7H-2	7H-6	8H-3	8H-4	8H-4	8H-5	8H-5	8H-6
Interval (cm)		63-65	68-70	24-26	139-141	129-131	146-148	10-Aug	34-36	60-62	7- 9	46-48	84-86
Cumulative volume percentages	Class interval (ϕ)												
	1.75-	0	0	0	0	0	0	0	0	0	0.7	0	0
	2.00-1.75	0	0	0	1.1	0	0	0	0	0	5	2.1	0
	2.25-2.00	0	0	0	2.8	0	0	0	0	0	11.3	5.3	0
	2.50-2.25	0	1.4	2	12.1	1.5	1.9	1.3	1.9	0.5	32.3	21.8	0
	2.75-2.50	0.4	5.7	7.5	22.9	5.9	7.4	5.1	7.2	3	52.2	38.7	0.3
	3.00-2.75	1.5	14.2	18.1	36.1	14.5	18.2	12.7	17.5	8.4	70.6	56.4	1
	3.25-3.00	7.4	29	32.8	49.3	28.4	34.5	25.9	32.3	23.2	81.7	70.1	6.1
	3.50-3.25	15.9	45.9	48.9	62.3	44.2	52.4	41.3	48.7	41.4	90	82	14.3
	3.75-3.50	32	62.6	63.8	72.9	59.9	67.7	58.2	64.2	60.8	93.2	88.8	33.9
	4.00-3.75	47	75.3	75.3	80.9	72.3	78.9	71.7	76	75.4	95.3	93.3	52
	4.25-4.00	61.1	84.3	83.7	86.6	81.5	86.1	82.1	84.4	85.6	96.3	95.7	68.6
	4.50-4.25	73.8	90.6	89.9	91	88.4	91.1	89.5	90.3	92.2	97.1	97.3	81.1
	4.75-4.50	83.3	94.3	93.9	93.9	92.8	94	94	93.8	95.8	97.6	98.1	89.1
	5.00-4.75	87.5	95.4	95.2	94.9	94.2	94.9	95.2	94.9	96.6	97.8	98.3	91.3
	5.00-6.00	94.6	97.3	97.3	97.2	96.6	96.7	97.2	96.9	97.9	98.5	98.9	94.7
	7.00-6.00	99.3	99.6	99.4	99.3	99	99	99.6	99.2	99.7	99.1	99.5	99.3

Table 3 (continued).

Site		790C	790C	790C	790C	790C	790C	790C	790C	790C	790C	790C	790C	790C
Core, section		3H-5	3H-6	5H-3	5H-5	5H-6	6H-2	6H-2	6H-3	6H-4	6H-4	6H-6	6H-6	7H-2
Interval (cm)		12-Oct	44-46	72-74	6-Apr	116-118	51-53	139-141	80-82	27-29	78-80	12-Oct	92-94	44-46
Cumulative volume percentages	Class interval (φ)													
	1.75-	0	0	0	0	0	0	0	0	0	0	0	0	0
	2.00-1.75	0	0	0	0.3	0	0	1.6	0	0	1.5	0	0	0
	2.25-2.00	0	0	0	0.8	0	0	4.1	0	0	3.9	0	0	0
	2.50-2.25	0	0	0.9	5.9	0	0	17.4	0.1	0	17	0	0.5	0
	2.75-2.50	0.6	0.6	3.9	14.8	0.7	0.8	31.6	1.5	1.1	31.7	0.9	2.7	0.7
	3.00-2.75	2.1	2.1	10	29.4	2.4	2.7	47.3	4.9	3.8	48.9	3.1	7.4	2.4
	3.25-3.00	9.6	9.6	22.5	45.2	10.8	11.7	60.6	16.9	15.3	63.3	12.9	20	10.4
	3.50-3.25	20.1	20.2	37.3	61.1	22.6	23.9	72.8	32.2	30.4	76.4	26.1	35.4	21.4
	3.75-3.50	37.8	38	52.8	73.4	42	42.6	80.9	50.2	49.9	84.4	45.2	52.5	38.3
	4.00-3.75	53.4	53.6	64.9	82.3	58.5	58.4	86.7	64.8	65.6	89.9	61.4	65.9	53.1
	4.25-4.00	67	67.2	73.9	88	72.3	71.5	90.3	76.2	77.8	93	74.8	75.8	66
	4.50-4.25	78.2	78.3	80.8	92	82.6	81.6	92.9	84.9	86.6	95.1	84.8	83.2	77.1
	4.75-4.50	86	86	85.4	94.3	89.2	88.3	94.5	90.6	92	96.3	91.1	87.9	85.2
	5.00-4.75	89.3	89.2	87.3	95.1	91.5	90.7	95.2	92.6	93.6	96.7	93	89.6	88.9
	5.00-6.00	95.1	95	92	97.1	95.5	95.1	97.1	96	96.2	97.8	96	93.8	95.4
	7.00-6.00	99.3	99.4	97.3	99.1	99.2	99.1	99.1	99.2	99.6	99.4	99.3	98.4	99.6

Site		790C	790C	790C	790C	790C	790C	790C	790C	790C	790C	790C	790C
Core, section		11X-2	11X-3	12X-1	12X-1	13X-1	13X-2	14X-2	16X-1	17X-7	18X-4	19X-1	20X-5
Interval (cm)		12-Oct	110-112	21-23	65-67	41-43	64-65	135-138	9- 11	29-31	121-123	94-96	20-22
Cumulative volume percentages	Class interval (φ)												
	1.75-	0	0	0	0	0	0	2.8	0	0	0	0	0
	2.00-1.75	0	0	0.5	0	1.4	0	10.6	0	0	0	0	1.7
	2.25-2.00	0	0	1.3	0	3.5	0	21.3	0	0	0	0	4.4
	2.50-2.25	0	1	7.7	0	15.3	1.2	32.8	0	1.1	0	0	18.2
	2.75-2.50	1.3	4.5	17.6	1	29	5	43.8	0	4.6	0	1.4	32.5
	3.00-2.75	4.5	11.7	32.8	3.5	45.4	12.6	54.1	0	11.8	0	4.8	47.8
	3.25-3.00	17.5	26.5	48.8	14.4	60.2	26.5	64.3	0	26	0	18.6	61
	3.50-3.25	34.2	43.9	64.7	28.9	74.1	42.7	74.5	0	42.7	0	36.2	73.3
	3.75-3.50	54.4	61.9	76.5	49	83.5	59.9	83.2	0	60.3	0	56.5	82.1
	4.00-3.75	70.3	75.5	85	65.9	90	73.3	89.6	0	73.8	0	72.3	88.4
	4.25-4.00	82.1	85.1	90.3	79.9	93.8	83	93.8	0	83.5	0	83.8	92.3
	4.50-4.25	90.2	91.5	93.9	89.8	96.2	89.9	96.6	0	90.2	0	91.5	95
	4.75-4.50	94.9	95.1	96	95.7	97.5	94	98.1	0	94.1	0	95.8	96.5
	5.00-4.75	96.1	96.1	96.6	97.1	97.9	95.2	98.6	0	95.2	0	96.8	97.1
	5.00-6.00	97.8	97.9	97.9	98.6	98.8	97.2	99.3	0	97.3	0	98.3	98.4
	7.00-6.00	99.7	99.9	99.4	99.7	99.7	99.3	99.9	0	99.8	0	99.8	99.6

Table 3 (continued).

Site		791A	791A	791A	791A	791A	791A	791A	791A	791A	791A	791A	791A	791A
Core, section		2H-5	4H-5	5H-2	5H-3	5H-4	6H-2	7H-2	10H-5	14H-4	18H-1	18H-1	30X-CC	33X-1
Interval (cm)		74-76	99-101	142-144	78-80	16-18	60-62	80-82	117-119	35-37	5- 7	53-55	18-20	50-52
Cumulative volume percentages	Class interval (ϕ)													
	1.75-	0	0	0	0	0	0	0	0	0	0	0	1.6	0
	2.00-1.75	0	0	0.7	0	0	0	0	0	0	0	0	7.1	0
	2.25-2.00	0	0	1.8	0	0	0	0	0.1	0	0	0	14.8	0.1
	2.50-2.25	0.6	0	8.9	2.5	0	0	0	2.8	1.7	0	0	29.3	3.2
	2.75-2.50	3	0.6	18.6	9.2	1	1	0.6	9.2	6.6	0.7	1	43.2	10.7
	3.00-2.75	8	2	32.1	22.1	3.5	3.4	2.2	21.1	16.1	2.4	3.4	56.4	24.7
	3.25-3.00	20.3	9.6	47	38.7	14.3	13.7	9.8	35.2	30.2	10.5	13.7	67	40.7
	3.50-3.25	35.5	20.5	62.2	56.3	28.6	27.2	20.4	50	45.9	21.8	27.1	76.6	57.2
	3.75-3.50	53.4	40.3	74.8	71.3	48.3	44.8	37.7	62.9	61.4	40.6	44.3	83.6	70.7
	4.00-3.75	68	57.8	84.1	82.2	64.7	59.9	53.4	72.9	73.6	56.9	58.6	88.7	80.8
	4.25-4.00	79.4	73.1	90.3	89.2	78	72.7	67.6	80.3	82.6	71	70.3	92.1	87.6
	4.50-4.25	87.9	84.7	94.4	93.8	87.7	83.1	79.4	85.9	89.3	81.6	79.4	94.4	92.4
	4.75-4.50	93.2	92.1	96.7	96.3	93.6	90.2	87.7	89.6	93.5	88.4	85.4	95.8	95.2
	5.00-4.75	94.8	94.3	97.3	97.1	95.3	92.7	90.9	91	94.8	90.5	87.5	96.3	96
	5.00-6.00	97.3	97	98.6	98.4	97.7	96.4	95.7	95	97	94.1	92.4	97.7	97.7
	7.00-6.00	99.8	99.6	99.8	99.8	99.7	99.3	99.3	98.7	99.3	98.7	97.6	99.3	99.5

Site		791A	791A
Core, section		39X-1	42X-1
Interval (cm)		90-92	31-33
Cumulative volume percentages	Class interval (ϕ)		
	1.75-	0	0
	2.00-1.75	0	0
	2.25-2.00	0	0
	2.50-2.25	1.4	1
	2.75-2.50	5.6	4.2
	3.00-2.75	13.8	10.7
	3.25-3.00	27.6	23.2
	3.50-3.25	43.4	38
	3.75-3.50	59.3	54.4
	4.00-3.75	71.8	67.6
	4.25-4.00	81	77.8
	4.50-4.25	87.9	85.6
	4.75-4.50	92.3	90.6
	5.00-4.75	93.8	92.4
	5.00-6.00	96.6	95.9
	7.00-6.00	99.4	99.1

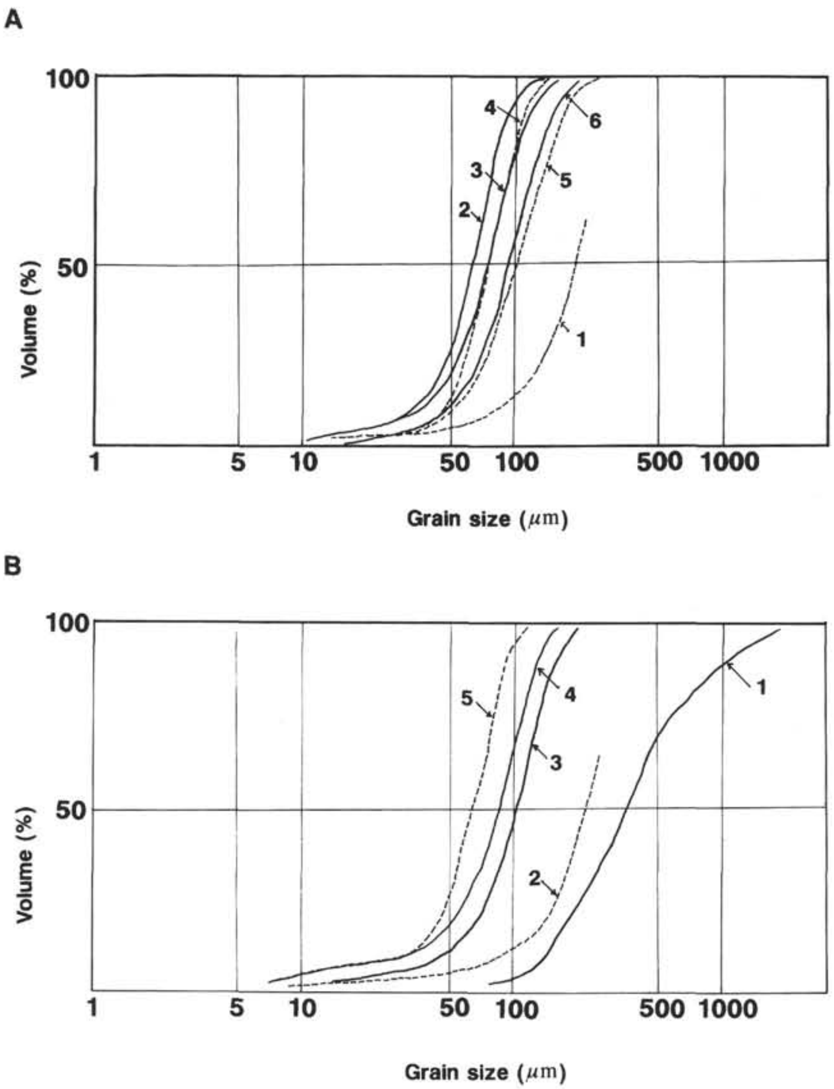

Figure 9. Cumulative grain-size distribution of the Quaternary volcanic ash layers. Grain sizes are indicated by microns (μm) in this diagram. **A.** Forearc Site 792. Broken lines indicate black ash layers and solid lines indicate white ash layers. (1) Sample 126-792B-8X-3, 60–62 cm; (2) Sample 126-792A-1H-1, 38–40 cm; (3) Sample 126-792A-8H-3, 40–42 cm; (4) Sample 126-792A-5H-2, 141–143 cm; (5) Sample 126-792A-4H-5, 19–21 cm; (6) Sample 126-792A-9H-4, 6–8 cm. **B.** Backarc Site 790. Broken lines indicate black ash layers and solid lines indicate white ash layers. (1) Sample 126-790B-5H-5, 43–47 cm; (2) Sample 126-790C-14X-2, 135–138 cm; (3) Sample 126-790C-5H-5, 4–6 cm; (4) Sample 126-790B-7H-6, 146–148 cm; and (5) Sample 126-790B-8H-6, 84–86 cm.

1965; Letouzey and Kimura, 1985). These tephras are distributed partly onshore and, for the most part, in submarine areas around the Philippine Sea.

ACKNOWLEDGMENTS

During Leg 126, Captain Ribbon and the crew of the *JOIDES Resolution* helped us, sometimes beyond the call of duty. These are warmly acknowledged. B. Taylor, J. Gill, R. Hiscott, and K. Marsaglia gave us valuable discussion and a warm understanding of the ashy sediments.

Thanks also go to Drs. M. Yuasa, S. Nagaoka, N. Kotake, Y. Hirata, and H. Matsuoka for their critical discussions on the tephras. Mrs. Kanehara and Miss K. Ikari and A. Koizumi helped us during the preparation of the manuscript.

REFERENCES

Brouxel, M., Lapierre, H., Michard, A., and Albarede, F., 1987. The deep layers of a Paleozoic arc: geochemistry of the Copley-Balaklala Series, northern California. *Earth Planet. Sci. Lett.*, 85:386–400.

Brown, G., and Taylor, B., 1988. Sea-floor mapping of the Sumisu Rift, Izu-Ogasawara (Bonin) Island Arc. *Bull. Geol. Surv. Jpn.*, 39:23–38.

Christiansen, R. L., and Lipman, P. W., 1972. Cenozoic volcanism and plate-tectonic evolution of the western United States. II. Late Cenozoic. *Philos. Trans. R. Soc. London, Ser. A*, 271:249–284.

Eaton, G. P., 1982. The Basin and Range Province: origin and tectonic significance. *Annu. Rev. Earth Planet. Sci.*, 10:409–440.

———, 1984. The Miocene Great Basin of western North America as an extending back-arc region. *Tectonophysics*, 102:275–295.

Fisher, R. V., 1984. Submarine volcaniclastic rocks. *In* Kokelaar, B. P., and Howells, M. F. (Eds.), *Marginal Basin Geology: Volcanic and Associated*

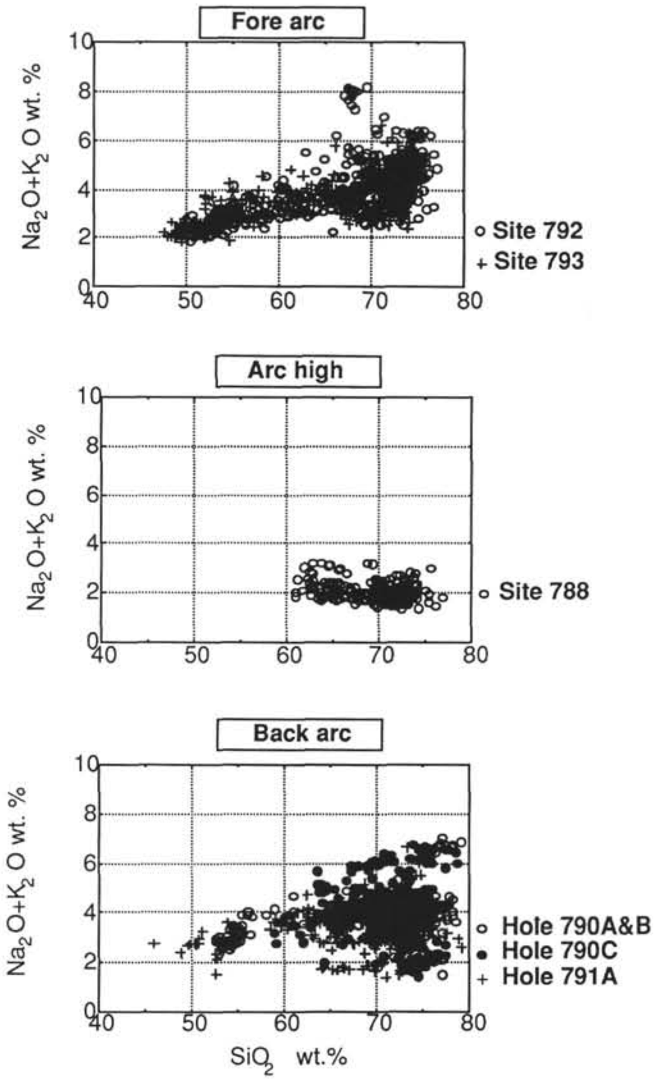

Figure 10. SiO_2-alkali diagram of the Quaternary volcanic ash layers at forearc Sites 792 and 793, arc Site 788, and backarc Sites 790/791.

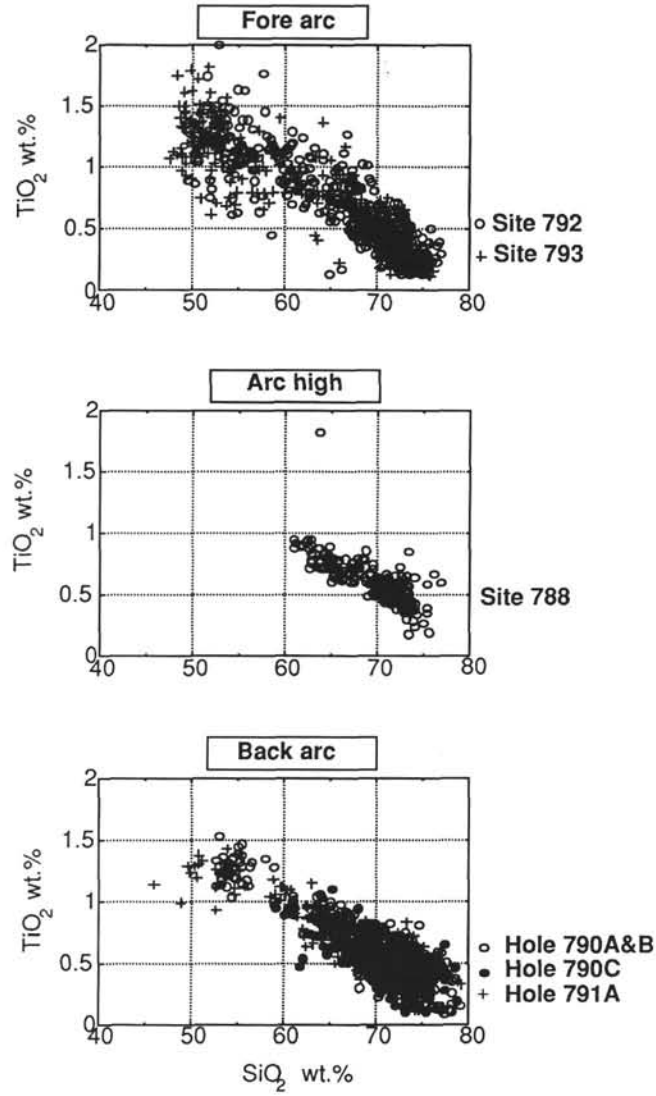

Figure 11. SiO_2-TiO_2 diagram of the Quaternary tephras at forearc Sites 792 and 793, arc Site 788, and backarc Sites 790/791.

Sedimentary Processes in Modern and Ancient Basins. Spec. Publ., Geol. Soc. London, 16:5–28.

Fiske, R. S., 1986. Shallow marine volcanic field in the Mio-Pliocene Shirahama Group, Izu Peninsula, Japan. *Geol. Soc. Am. Abstr. Programs,* 1986 Annual Meeting, 602.

Fiske, R. S., and Cashman, K. V., 1989. Submarine fallout deposit in the Shirahama Group (Mio-Pliocene), Japan. *Abstr. Vol., Int. Assoc. Volcanol. Chem. Earth's Interior, Gen. Assem.,* Santa Fe, New Mexico, No. 92.

Fujioka, K., 1983a. History of the explosive volcanism of the Tohoku Arc from the core sediment samples of the Japan Trench. *J. Volcanol. Soc. Jpn.,* 28:41–58.

————, 1983b. Where were the "Kuroko deposits" formed, looking for the present day analogy. *Min. Geol. (Tokyo), Spec. Vol.,* 11:55–68.

————, 1988. A possible nascent rift in northern Izu-Ogasawara arc. *In Tectonics of Eastern Asia and Western Pacific Continental Margin.* 1988 DELP Tokyo Int. Symp. and Sixth Japan-U.S.S.R. Geotectonic Symp., 25. (Abstract)

Fujioka, K., Furuta, T., and Arai, F., 1980. Petrography and geochemistry of volcanic glass: Leg 57, Deep Sea Drilling Project. *In* von Huene, R., Nasu, N., et al., *Init. Repts. DSDP,* 56, 57, Pt. 2: Washington (U.S. Govt. Printing Office), 1049–1066.

Fujioka, K., Nishimura, A., Koyama, M., and Kotake, N., 1990. Bimodal arc volcanism and backarc rifting along Izu-Bonin Arc. *Eos,* 71:956.

Furuta, T., and Arai, F., 1980a. Petrographic and geochemical properties of tephras in Deep Sea Drilling Project cores from the north Philippine Sea. *In* Klein, G. de V., Kobayashi, K., et al., *Init. Repts. DSDP,* 58: Washington (U.S. Govt. Printing Office), 617–627.

————, 1980b. Petrographic properties of tephras, Leg 56, Deep Sea Drilling Project. *In* von Huene, R., Nasu, N., et al., *Init. Repts. DSDP,* 56, 57, Pt. 2: Washington (U.S. Govt. Printing Office), 1043–1048.

Furuta, T., Fujioka, K., and Arai, F., 1986. Widespread submarine tephra around Japan, petrographic and chemical property. *Mar. Geol.,* 72:125–146.

Gill, J. B., 1981. *Orogenic Andesites and Plate Tectonics:* New York (Springer-Verlag).

Gill, J. B., Stork, A. L., and Whelen, P. M., 1984. Volcanism accompanying backarc basin development in the Southwest Pacific. *Tectonophysics,* 102:207–224.

Gill, J., Torssander, P., Lapierre, H., Taylor, R., Kaiho, K., Koyama, M., Kusakabe, M., Aitchison, J., Cisowsky, S., Dadey, K., Fujioka, K., Klaus, A., Lovell, M., Marsaglia, K., Pezard, P., Taylor, B., and Tazaki, K., 1990. Explosive deep water basalt in the Sumisu backarc rift. *Science,* 248:1214–1217.

Hawkins, J. W., and Melchior, J. T., 1985. Petrology of Mariana Trough and Lau Basin basalts. *J. Geophys. Res.,* 90:11431–11468.

Hochstaedter, A. G., Gill, J. B., Kusakabe, M., Newman, S., Pringle, M., Taylor, B., and Fryer, P., 1990a. Volcanism in the Sumisu Rift. I. Major

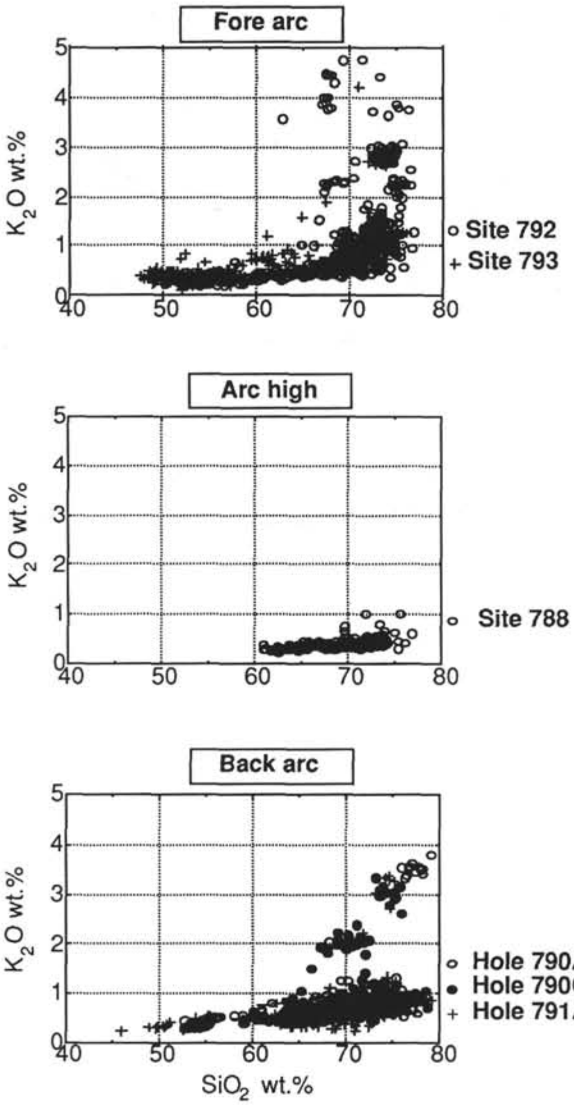

Figure 12. SiO_2-K_2O diagram of the Quaternary tephras at forearc Sites 792 and 793, arc Site 788, and backarc Sites 790/791.

element, volatile, and stable isotope geochemistry. *Earth Planet. Sci. Lett.*, 100:179–194.

Hochstaedter, A. G., Gill, J. B., and Morris, J. D., 1990b. Volcanism in the Sumisu Rift. II. Subduction and non-subduction related components. *Earth Planet. Sci. Lett.*, 100:195–209.

Ikeda, Y., and Yuasa, M., 1989. Volcanism in nascent back-arc basins behind the Shichito Ridge and adjacent areas in the Izu-Ogasawara arc, northwest Pacific: evidence for mixing between E-type MORB and island arc magmas at the initiation of back-arc rifting. *Contrib. Mineral. Petrol.*, 101:377–393.

Inmann, D. L., 1952. Measures of describing the size distribution of sediments. *J. Sediment. Petrol.*, 22:125–145.

Kennett, J. P., MacBirney, A. R., and Thunell, R. C., 1979. Episodes of Cenozoic volcanism in the circum-Pacific region. *J. Volcanol. Geotherm. Res.*, 2:145–163.

Table 4. Chemistry of volcanic glass shards, Sites 788, 790/791, and 792/793.

Site	SiO_2	TiO_2	K_2O	Na_2O	Total alkali
790/791	65%–80%	0.1%–1.0%	0.5%–4.0%	1.0%–6.0%	1.7%–7.0%
788	70%–80%	0.3%–1.0%	0.2%–0.7%	1.3%–2.7%	1.7%–3.0%
792/793	65%–80%	0.1%–1.0%	0.2%–4.5%	1.6%–4.7%	2.5%–8.4%

Kokelaar, B. P., Bevins, R. E., and Roach, R. A., 1985. Submarine silicic volcanism and associated sedimentary and tectonic processes, Ramsey Islands, SW Wales. *Geol. Soc. London,* 142:591–613.

Konishi, K., 1965. Geotectonic framework of the Ryukyu Islands (Nansei-shoto). *J. Geol. Soc. Jpn.,* 71:437–457.

Kotake, N., 1988. Upper Cenozoic marine sediments in southern part of the Boso Peninsula, central Japan. *J. Geol. Soc. Jpn.,* 94:187–206.

Kuno, H., 1966. Lateral variation of basalt magma type across continental margins and island arcs. *Bull. Volcanol.,* 19:195–222.

Leg 126 Scientific Drilling Party, 1989. ODP Leg 126 drills the Izu-Bonin Arc. *Geotimes,* 34:36–38.

Leg 126 Shipboard Scientific Party, 1989. Arc volcanism and rifting. *Nature,* 342:18–20.

Letouzey, J., and Kimura, M., 1985. Okinawa trough genesis: structure and evolution of a backarc basin developed in a continent. *Mar. Pet. Geol.,* 2:111–130.

Machida, H., and Arai, F., 1983. Extensive ash falls in and around the sea of Japan from large late Quaternary eruptions. *J. Volcanol. Geotherm. Res.,* 18:151–164.

————, 1988. A review of late Quaternary deep-sea tephras around Japan. *Quart. Res.,* 26:227–242.

Miyashiro, A., 1974. Volcanic rock series in island arcs and active continental margins. *Am. J. Sci.,* 274:321–355.

Murakami, F., 1988. Structural framework of the Sumisu Rift, Izu-Ogasawara Arc. *Bull. Geol. Surv. Jpn.,* 39:1–21.

Nakamura, K., 1964. Volcano-stratigraphic study of Oshima Volcano, Izu. *Bull. Earthquake Res. Inst., Univ. Tokyo,* 42:649–728.

Nishimura, A., and Murakami, F., 1988. Sedimentation of the Sumisu Rift, Izu-Ogasawara Arc. *Bull. Geol. Surv. Jpn.,* 39:39–61.

Omura, A., 1984. Radio-isotope of uranium and thorium. *Earth Monthly,* 6:523–528.

Reagan, M. K., and Meijer, D., 1984. Geology and geochemistry of early sea-volcanic rocks from Guam. *Bull. Geol. Soc. Am.,* 95:701–713.

Sparks, R.S.J., Wilson, L., and Sigurdsson, H., 1981. The pyroclastic deposits of the 1875 eruption of Askja, Iceland. *Philos. Trans. R. Soc. London, Ser. A,* 299:241–273.

Takada, A., Oshima, O., Aramaki, S., Ono, K., Yoshida, T., and Kajima, K., in press. Geology of Aogashima Volcano, Izu Islands, Japan. *Bull. Volcanol. Soc. Jpn.*

Taylor, B., Fujioka, K., et al., 1990. *Proc. ODP, Init. Repts.,* 126: College Station, TX (Ocean Drilling Program).

Walker, G.P.L., 1971. Grain size characteristics of pyroclastic deposits. *J. Geol.,* 79:696–714.

Yamazaki, T., 1988. Heat flow in the Sumisu Rift, Izu-Ogasawara (Bonin) Arc. *Bull. Geol. Surv. Jpn.,* 39:63–70.

Yokoyama, T., Danhara, T., and Yamashita, T., 1986. A new refractometer for volcanic glass. *J. Volcanol. Soc. Jpn.,* 25:21–30.

Date of initial receipt: 2 January 1991
Date of acceptance: 22 October 1991
Ms 126B-116

Table 5. Correlation of marine tephras by mineral assemblage, chemistry, glass type, refractive indices, and age of the volcanic ash layers.

Core,section, interval (cm)	1)	792A-3H-1, 86-88	793A-4H-2, 96-98	2)	792A-5H-3,131-133	442A-5-3,30-34*
Age		CN14b	CN14b-a		CN14a	*p.lacunosa*
R.I.(Mean)		1.5067	1.5067		1.5013	1.501-1.504
R.I.(Range)		1.5058-1.5080	1.504-1.5047		1.4998-1.5024	1.500-1.505
Mineral assemblage		pl++,hb+	pl++,hb+		pl++,cpx+,hb+,op+	pl+,hb
Glass shape		bw	bw		bw	
Thickness (cm)		14 (ML)	Dispersed in mud		90 (ML)	
Glass grain size(Max)		0.25	0.15		0.2	0.2
Mode		95/5/0	94/5/1		95/5/0	

Core,section, interval (cm)	3)	792B-1H-1,50-52	Kurasaki volcano	4)	792A-1H-5,81-83	Aso-4**
Age		CN15			CN15	80,000B.P.
R.I.(mean)		1.5065			1.5096	
R.I.(range)		1.5056-1.5073			1.509-1.5108	1.506-1.514
Mineral assemblage		pl++			pl++,cpx+,hb+,op+	pl,hb,opx,cpx
Glass shape		bw			bw	bw>>pum
Thickness (cm)		7			3	
Glass grain size(Max)		0.05			0.55	
Mode					93/5/2	

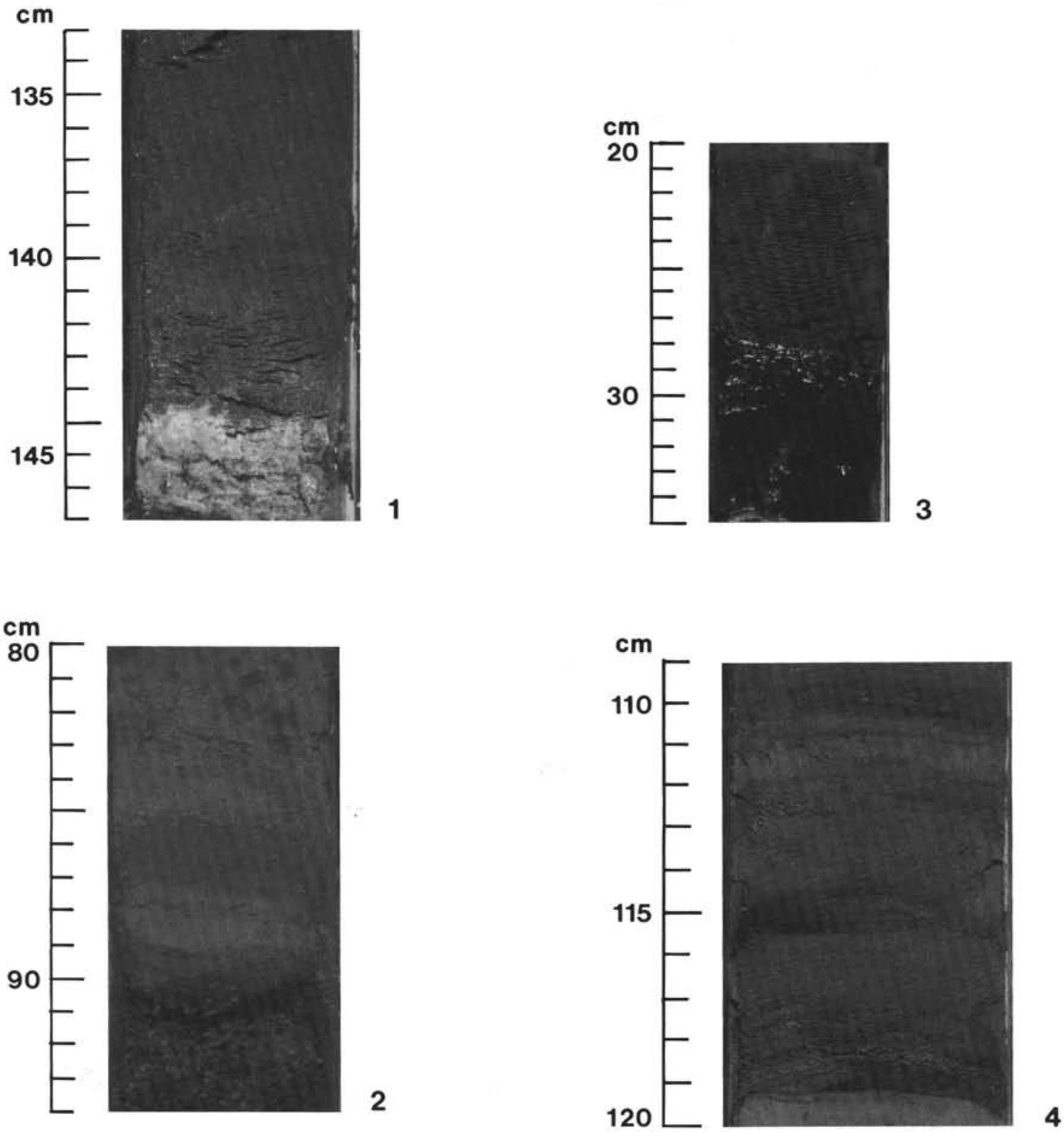

Plate 1. Core photographs. **1.** Sample 126-790B-7H-6, 145–148 cm, simple white volcanic ash layer. **2.** Section 126-792A-3H-1, 80–94 cm, multiple ash layers with crystal-rich, coarse black ash at the bottom and 10 cm of thick, gray, mixed-ash layer above the black ash. **3.** Section 126-790C-5H-5, 20-35 cm. multiple black ash layers with fine, sandy ash in the bottom of the tripartite (Taylor, Fujioka, et al., 1990). **4.** Section 126-793A-7H-2, 109–120 cm, sharp-based, parallel-laminated, mixed volcanic-ash layer with notable grading structure inside (Taylor, Fujioka, et al., 1990).

1 1 mm

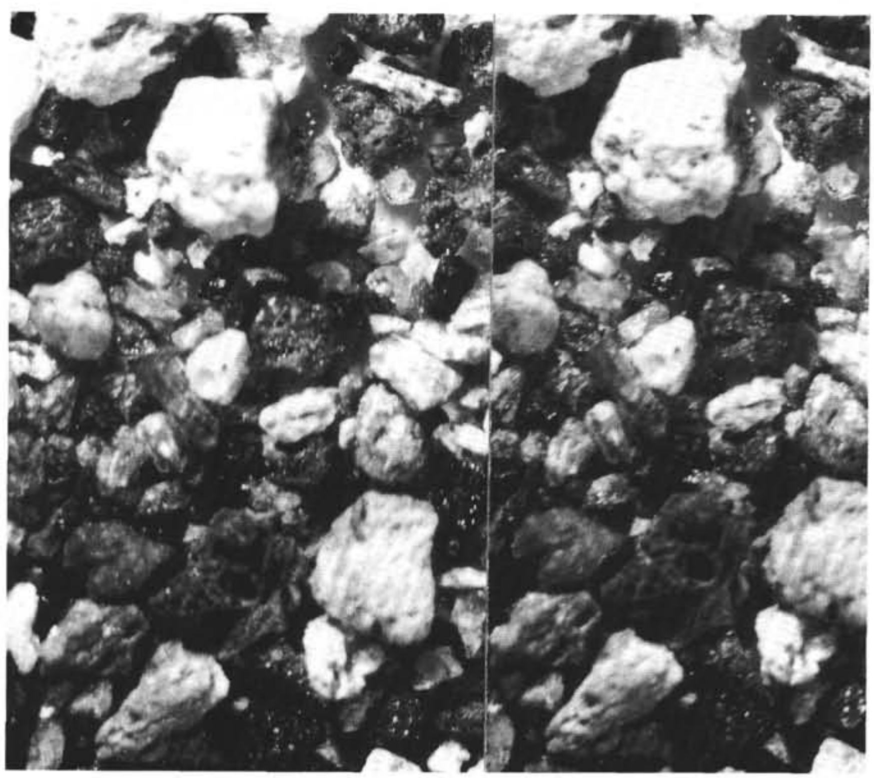

2 1 mm

Plate 2. Stereographic photographs of the volcanic ash layers. **1.** Sample 126-791A-10H-5, 117–119 cm, example of poorly sorted coarse white pumice. **2.** Sample 126-793A-1H-2, 118–120 cm, example of mixed volcanic glass shards, consisting of white and dark gray pumices and scoria.

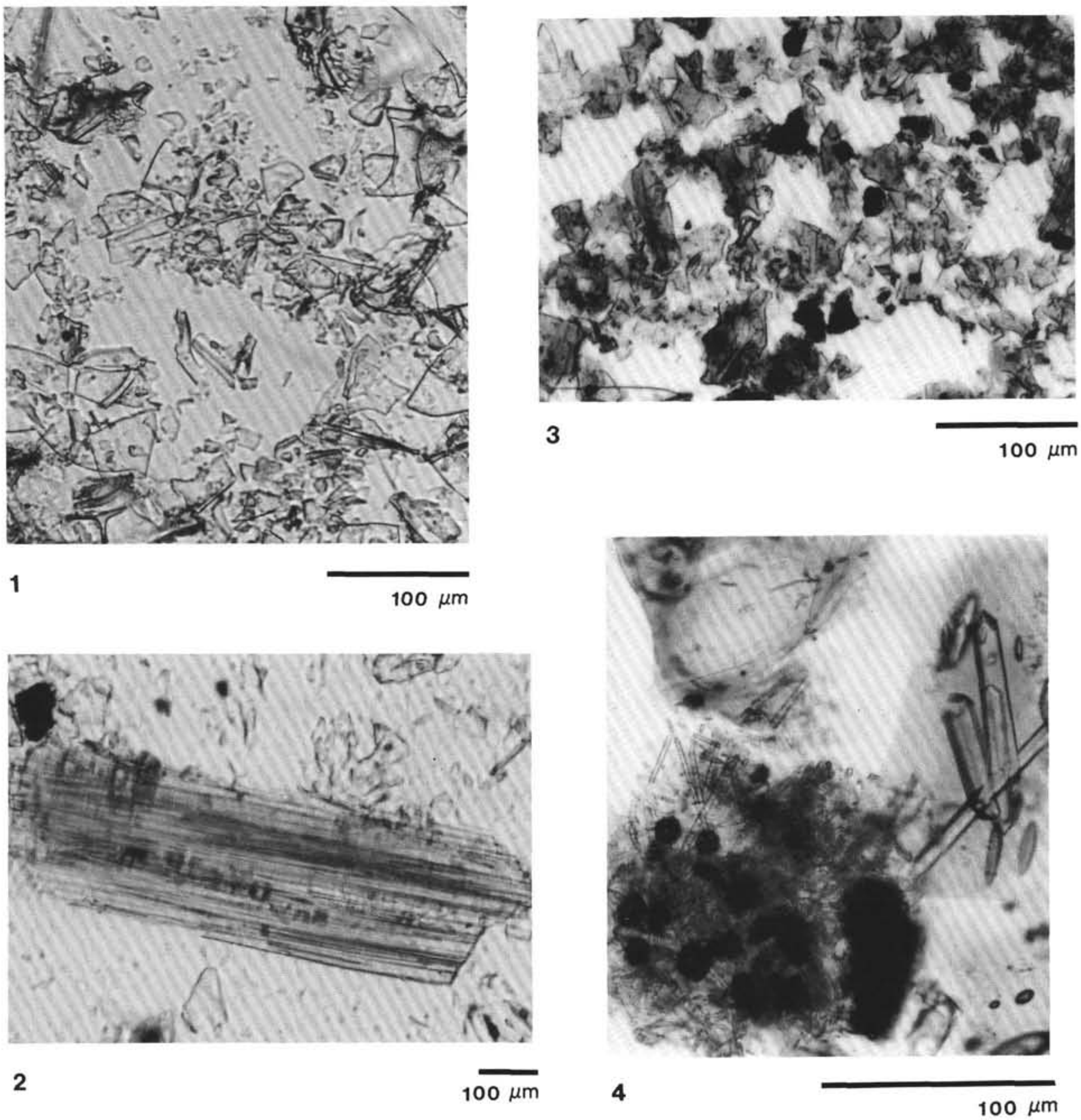

Plate 3. Photomicrographs of smear slides of the volcanic ash layer. **1.** Sample 126-793A-7H-3, 35–37 cm, fine, white, bubble-wall-type glass shards. **2.** Sample 126-792A-1H-6, 119–121 cm, tabular volcanic glass shards in the coarse, white tephra. **3.** Sample 126-793A-8H-5, 28–30 cm, brown glass in the fine, black tephra. **4.** Sample 126-792A-6H-3, 130–132 cm, crystallized brown volcanic glass in the coarse black tephra.